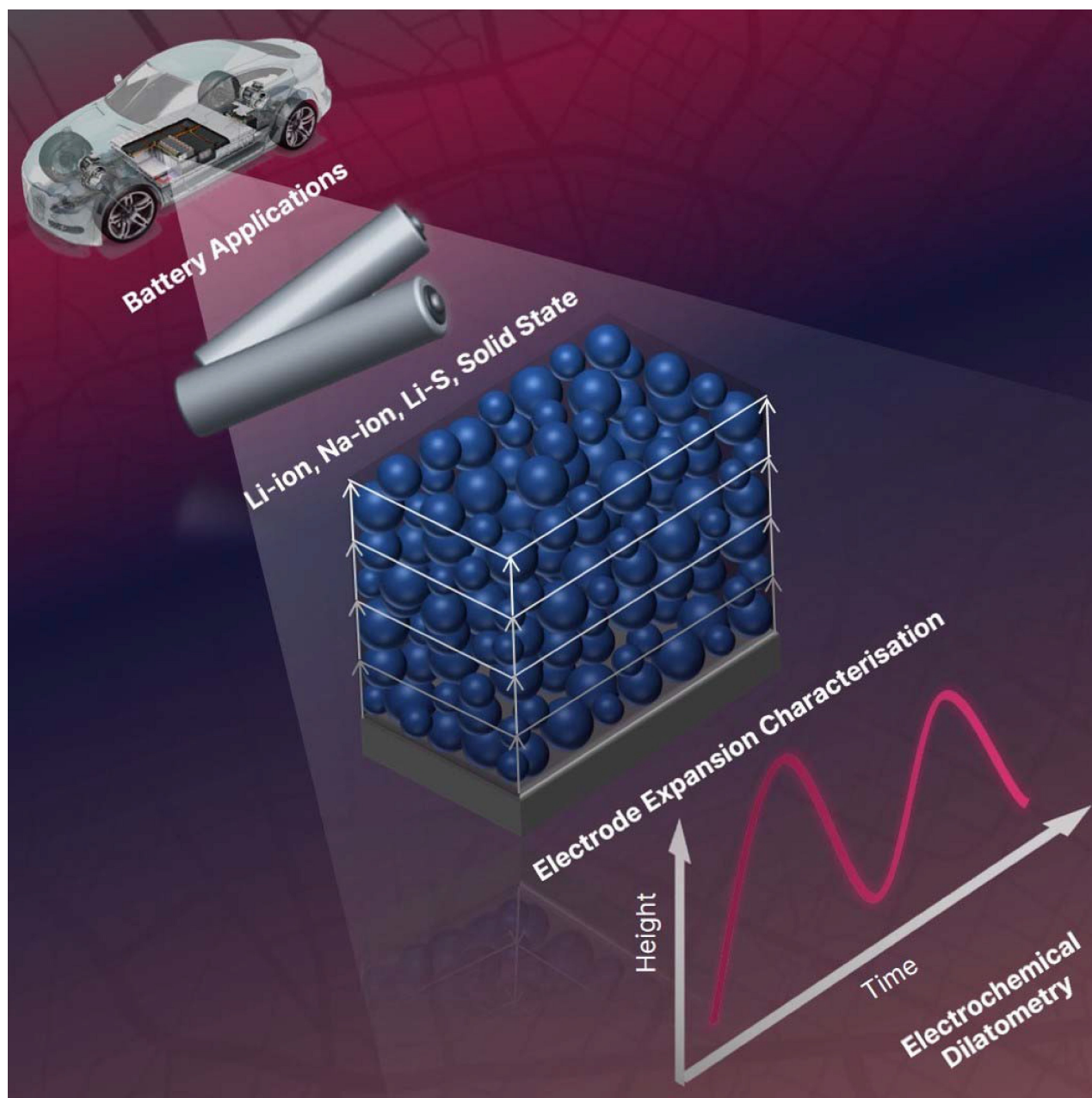Special Collection

Developments in Dilatometry for Characterisation of Electrochemical Devices

Harry Michael,[a] Rhodri Jervis,[a, b] Dan J. L. Brett,[a, b] and Paul R. Shearing*[a, b]

Since the 1970s, electrochemical dilatometry (ECD) has been used to investigate the dilation of layered host materials due to the intercalation of guest ions, atoms or molecules, and has recently gained traction in application to various electrochemical devices, such as lithium-ion batteries (LiBs), which have electrodes that undergo volume changes during cycling, resulting in particle cracking and electrode degradation. With resolution capabilities spanning tens of microns down to a few nanometres, dilatometry is a valuable tool in understanding how commonly used electrodes dilate and degrade and can therefore be of critical value in improving their performance. In recent years, there has been a plethora of studies using dilatometry as a monitoring tool for understanding operating performance in various electrochemical devices; however, to our knowledge, there has been no in-depth review of this body of research to date. This paper seeks to address this by reviewing how dilatometry works and how it has been used for the characterisation of electrochemical energy storage devices.

1. Introduction

The exploitation of carbon intensive fuels has contributed to a rise in global air pollution and global warming. As a result, the international community has developed strategies that reduce our reliance on these fuels and explore alternative means of providing energy.[1] This includes expanding research into various electrochemical devices.[2,3] Lithium-ion batteries (LiBs), sodium-ion batteries (NiBs), lithium sulfur (Li—S) batteries and solid-state batteries (SSBs) provide promising potential in meeting the needs of a diverse range of energy-intensive applications. Each electrochemical device varies across a spectrum of properties, such as energy density, cycle life, size and durability, rendering it uniquely suited to specific tasks.

Recent research has focussed on the understanding of materials and devices under operando conditions,[4–7] one tool that can make a contribution to this is electrochemical dilatometry (ECD), which has found increasing application in energy materials research in recent years. This review will outline the working principles of dilatometry measurements and survey ECD's application to a range of electrochemical devices.

1.1. Electrochemical Devices

Here, we briefly establish the working principles for the electrochemical devices considered.

[a] H. Michael, Dr. R. Jervis, Prof. D. J. L. Brett, Prof. P. R. Shearing
The Electrochemical Innovation Lab
Department of Chemical Engineering
University College London
WC1E 7JE, London, United Kingdom
E-mail: P.Shearing@ucl.ac.uk

[b] Dr. R. Jervis, Prof. D. J. L. Brett, Prof. P. R. Shearing
The Faraday Institution, Quad One
Harwell Science and Innovation Campus
Didco, OX11 0RA, United Kingdom

1.1.1. Rechargeable Metal-Ion Battery Chemistries

A metal-ion battery consists of four main components: anode, cathode, separator and electrolyte. During discharge, such batteries create an electron flow, which can be used to power a variety of devices. The negative electrode (often termed the anode as it undergoes oxidation during the galvanic process of discharge) and positive electrode (often termed the cathode as it undergoes reduction during discharge) are constructed of two dissimilar materials which accommodate the oxidation and reduction reactions, respectively. The electrolyte provides a medium for ions to flow between the respective electrodes enabling charge balance to complete the oxidation/reduction process. The purpose of the separator is to allow ions to flow and ensure the anode and cathode do not electrically short circuit. During operation, the electrodes typically dilate or contract. During charge, the anode either intercalates or alloys with metal-ions (depending on the electrode composition), whilst the cathode deintercalates metal ions causing it to decrease in thickness. Generally, alloying reactions cause more severe morphological changes and so thickness variations occur at a far larger scale in these systems (Si, Sn, Ge etc). The properties of a battery, such as its capacity, current capability, cycle life, safety, storage life, operating temperature and voltage, are determined by the materials used to construct the anode, cathode and electrolyte and its operating parameters. The lithium-ion battery (LiB), sodium-ion battery (NiB) and potassium-ion battery are all examples of metal-ion batteries. The lithium solid-state battery (SSB) is a metal-ion battery that employs a solid electrolyte material. Solid-state electrolytes are generally composed of inorganic Li-ion conductors, polymer electrolytes and organic–inorganic hybrid composites.[8]

1.1.2. Lithium-Sulfur (Li—S) Battery

The Li—S battery utilizes a cathode that is composed of elemental sulfur and carbon and an anode composed of elemental Li. The electrodes are separated by a separator soaked in organic electrolyte. Redox reactions take place between metallic Li and elemental sulfur.[9,10] A Li—S battery offers a theoretical capacity of up to 1672 mAh g^{-1} and an energy density of 2600 Wh Kg^{-1}, which corresponds to a 3–5 fold higher theoretical energy density than current state-of-the-art LiBs.[11] However, Li—S batteries are severely hampered by

Batteries & Supercaps

Reviews
doi.org/10.1002/batt.202100027

Chemistry Europe
European Chemical
Societies Publishing

practical hurdles that include short cycle life, low cycling efficiency, poor safety and a high self-discharge rate.[12,13] Dissolution of metallic lithium occurs at the anode surface, producing electrons and lithium ions during discharge and electrodeposition during charge. During discharge, dissolved lithium ions are incorporated into alkali metal polysulfide salts and the dissolved lithium ions migrate to the sulfur electrode (cathode) where sulfur is reduced to lithium sulphide. Therefore, sulfur is re-oxidised during discharge.[14,15]

Huge volumetric changes occur when sulfur (2.07 g cm^{-3}) is reversibly converted into lithium sulphide (Li$_2$S) (1.66 g cm^{-3}) via soluble lithium polysulfides during lithiation and delithiation. The soluble polysulfides may shuttle between the anode and cathode (shuttle effect) and form Li$_2$S$_2$ or Li$_2$S solid on the lithium anode. Deposition of Li$_2$S leads to 80% volume expansion compared to solid S$_8$.[16,17] In addition, cumulative volume changes in the sulfur electrode will occur as a result of the incomplete conversion of Li$_2$S and associated polysulfides to S upon recharging of the cell.[12] These mechanisms are assumed to be the major source of volume change in Li–S batteries.[18]

1.2. The Working Principles of a Dilatometer

A dilatometer measures volume changes of a sample material caused by chemical or physical processes. Dilatometry is typically used to test a wide range of materials, including metals, carbonaceous materials, ceramics, glasses and polymers.[19] There are different types of dilatometers: push-piston dilatometers; capacitance dilatometers; push rod dilatometers; high resolution-laser dilatometers; and optical dilatometers. This review focusses mostly on studies that use a push-piston dilatometer as this is the most commonly selected type of dilatometer for electrochemical devices, probably owing to the spatial resolution of commercially available models. That said, it should be noted that in SSB research, the push rod dilatometer is more common because it can operate at temperatures exceeding 1000 °C; most commercial push-piston dilatometers cannot operate at temperatures above 100 °C and tend to be used in studies carried out at room temperature. Use of the push rod dilatometer is discussed further in section 2.3. For multi-point expansion measurements using a laser dilatometer see the work of Spingler et al.[20] and for non-contact volumetric measurements using an optical dilatometer see the work of Bohn et al.[21]

Push-piston dilatometers use a parallel plate capacitor, with one stationary plate, and one mobile plate. When the sample material expands or shrinks, the mobile plate moves, which alters the gap between the two plates.[22–25] Push-piston dilatometers are designed to measure either horizontal or vertical displacement at a single point in 1-dimension.

There are various dilatometer instruments designed to measure electrochemical devices that are sealed against ambient temperature and pressure, and dilatometer cells can be designed to allow for gas expansion from the electrode in the electrochemical device. Commercially available push-piston dilatometers are often designed in a way to allow for gas evolution to be mitigated and thus not effect dilatometric measurements, so that dilation recorded is indicative of structural changes in the sample material. Pressiometry can be employed to monitor pressure changes in a sample material during cycling.[26,27] Numerous commercial pressiometry devices such as the PAT-Cell Press provided by EL-Cell group are built in a way that allow for the gas formed to be collected and transferred for subsequent gas analysis, e.g., gas chromatography. This allows measurements of gases formed during certain cycling protocols of different materials.

Linear voltage displacement transducers (LVDTs) and capacitive parallel-plate displacement sensor systems are the

Harry Michael received his M. Sci. for Electrochemistry and B. Sc. for Chemistry from the University of Southampton. He is currently a Ph.D. candidate in the Department of Electrochemical Engineering at UCL, United Kingdom under the supervision of Prof. Paul Shearing. His research interests include the degradation of Li-ion batteries and is affiliated with the Faraday Institution.

Rhodri Jervis is a lecturer at University College London. He Obtained his Ph.D. in fuel cell catalysis at University College London in 2015. His research interests lie in the advanced characterisation of materials for energy devices and is the project lead of The Faraday Institution's Degradation project.

Dan Brett is a professor of Chemical Engineering at UCL. His research interests lies in electrochemical energy conversion and storage, electrochemical sensors; electroanalysis, hybrid vehicles and micro-generation technologies. He is also active in modelling, instrumentation development, engineering design, device fabrication, materials development, and techno-economic analysis of electrochemical energy conversion technologies.

Paul Shearing is a professor of Chemical Engineering at UCL and Royal Academy Engineering Chair in Emerging Battery technologies. His research interests lies in the design of electrochemical processes in devices including fuel cells, batteries, and electrochemical reactors. He is involved in a wide range of projects which includes the understanding and development of batteries, fuel cells and other electrochemical processes and leads the LiSTAR project under the auspices of The Faraday Institution.
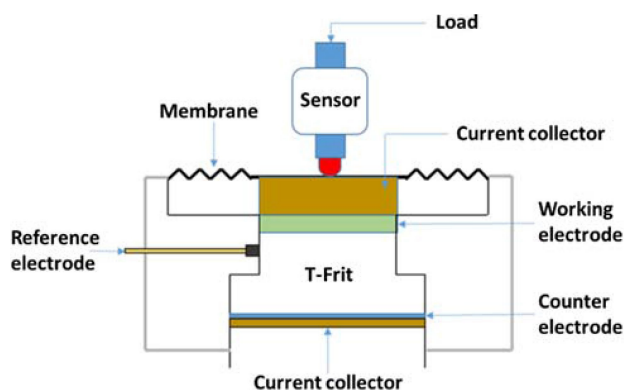
Batteries & Supercaps

Reviews
doi.org/10.1002/batt.202100027

Chemistry Europe
European Chemical
Societies Publishing

Figure 1. A figure detailing the internal mechanism of the ECD-3-Nano Dilatometer (by EL-Cell GmbH) based on a 3-electrode geometry and an inductive sensor. Only the dilatation of the WE is recorded because the glass T-frit is fixed in position. Adapted from Ref. [33] under the Creative Commons License. Copyright (2021) The Authors.

Figure 2. a) A schematic of the in-house developed dilatometer used by Hahn et al.[28] and b) by Winter et al.[29] Reproduced from Refs. [28] and [29] with permission. Copyright (2006) Springer-Verlag, (2000) The Electrochemical Society, respectively.

two most commonly found in numerous dilatometer instruments. Whilst there are multiple examples of in-house developed dilatometers designed for volumetric measurements,[28–32] commercially available instruments, such as the ECD model cells provided by EL-Cell group, GmbH are the most widely applied (see Figure 1).

It is noteworthy that this commercial cell can also be used for two-electrode cell configurations by replacing the reference electrode with a plug ferrule. In addition, The ECD-3-nano can be used to measure the expansion of a whole cell stack (instead of just the electrode on top of the frit). In this scenario, the glass frit is being replaced by a stainless-steel support. The cell stack components consist of the negative electrode, separator and positive electrode. This alternative dilatometer assembly is also suitable for solid-state batteries.[161]

Whilst a number of reports cited in this review used a version of a commercially available ECD dilatometer, it is also common to construct a tailored assembly to suit the purpose of the experiment. For instance, Hahn et al. constructed an in-house developed dilatometer that consisted of a two-electrode assembly with a paper separator (see Figure 2a). The lower counter electrode (CE) was fixed into position while the upper working electrode had freedom to move against a constant load (20 N) applied by a spring. An inductive displacement transducer and a measuring amplifier were used to record the height changes of the cell. The transducer and measuring amplifier were mounted on top of a plunger that connect the detector to the working electrode (WE). A drying agent was connected to the cell to prevent pressure increases due to gas evolution.

Figure 2b illustrates the dilatometer developed by Winter et al.[29] They used the resonance frequency shift in an oscillatory circuit that contains two ferrite shells. One of the ferrite shells was mounted so that it was mobile. The WE was placed between two pistons. Nickel was used to make the bottom piston, which was stationery and functioned as the current collector. Polypropylene (PP) was used to make the upper piston, which was allowed to move and transmit
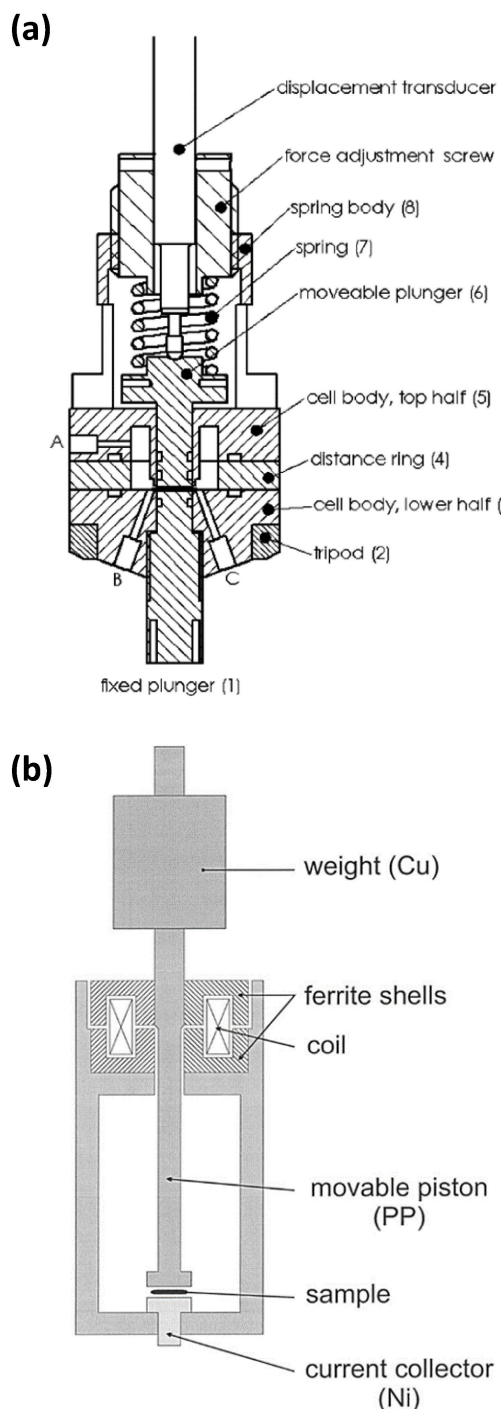
thickness changes in the WE to the upper ferrite shell of the oscillatory circuit. Some design limitations were observed; capillary forces allowed electrolytic solution to move between the WE and piston producing false expansion measurements. In addition, electrolyte creeped between the sample and Ni current collector, disrupting electronic contact between the current collector and sample, and leading to measurements

Batteries & Supercaps

Reviews
doi.org/10.1002/batt.202100027

Chemistry Europe
European Chemical
Societies Publishing

being entirely aborted. This issue of electrolyte creeping was resolved by installing a small copper weight into the dilatometer apparatus to ensure contact between the nickel current collector (bottom piston), WE (sample) and upper piston was maintained.[29]

The dilatometry set-up used by Ivanov et al. included an electrode stack, which consisted of an anode coating on one side, and a cathode on the opposite with a separator in between (see Figure 3a). The three constituents of the electrode stack could be homogenously pressed by bracing the spring with a force adjustment screw to ensure a homogeneous mechanical pressure is applied to the cell. Electrode expansion was monitored by using the displacement sensor and the macroscopic electrode stress by the load cell.[34] As a result of the increased length of the pressure spring in comparison to the displacement of the electrodes caused by swelling, force changes during measurements were negligible. In addition, the effect of gas evolution during cycling was suppressed owing to the small electrode area, the applied compression, and the non-gas tight housing. Bauer et al. also measured the expansion of a whole cell using an in-house developed dilatometer.[31] The height changes of the cell were transmitted via a membrane and a piston onto a LVDT. A voltage output was produced, which varied linearly according to the cell's expansion (see Figure 3b). The in-house constructed load system used for ECD measurements by Jeong et al. consisted of a sandwich-type electrode stack with a spring component.[32] A gap-sensor (resolution: 0.5 μm) was used to measure the thickness changes of the electrode stack (see Figure 3c).

Numerous studies use dilatometry in tandem with other electrochemical techniques to provide more information on the electrochemical device in question. For instance, Winter et al. used cyclic voltammetry to assess the feasibility of electrolytic solutions with graphite in rechargeable cells that were subsequently used for ECD measurements.[29] The study set out to monitor electrolyte penetration into pores or fissures of an exfoliated sample. However, they found that combining ECD with cyclic voltammetry caused cyclic voltammograms to be strongly affected by background currents in the dilatometer apparatus, demonstrating the limitations of combining these techniques. The dilatometer used in this work is shown in Figure 2b. It is common for dilatometry measurements to be taken with the entire experimental setup in a climate chamber so that conditions can be controlled during data acquisition and dimensional changes caused by certain temperatures can be assessed.

Other examples of studies that use in-house constructed dilatometers are discussed throughout this review. Most in-house dilatometer assemblies follow the same principles as those discussed in this section, with some adjustments. For example, studies by Fu et al.[35] and Bauer et al.[36] used two LVDTs because of the vertical alignment of the pouch cell in the designed fixture. One LVDT was placed on either side of the battery allowing the measurement of thickness variations at two different locations of the cell.
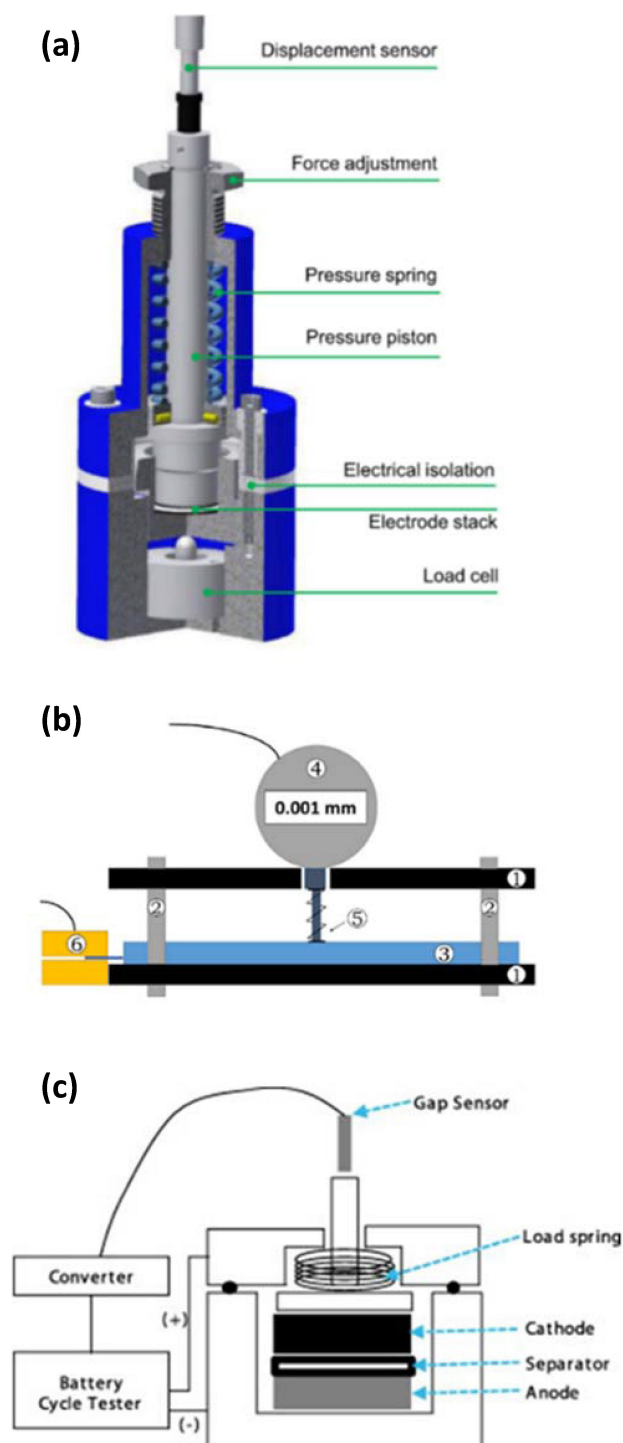
Figure 3. a) A schematic of the in-house developed dilatometer used by Ivanov et al. Reproduced from Ref. [30] with permission. Copyright (2017) Elsevier. b) The in-house developed dilatometer used by Bauer et al. for high-rate dilatometry experiments using GITT. Reproduced from Ref. [31] with permission. Copyright (2016) Elsevier. The dilatometer set-up consists of a (1) Al- plate (2) threaded rod (3) cell (4) dial gauge (5) tip with spring and metallic plate (1 cm²) (6) electric contact pads (gold plated). c) The lab-generated load cell system used for dilatometric studies by Jeong et al. Reproduced from Ref. [32] with permission. Copyright (2011) Elsevier.

Batteries & Supercaps

Reviews
doi.org/10.1002/batt.202100027

Chemistry
Europe
European Chemical
Societies Publishing

2. Application to Electrochemical Devices

2.1. Dilatometric Characterisation of LiBs

2.1.1. Overview

Understanding how commonly adopted electrodes dilate and contract in LiBs using ECD can be of critical value in improving LiB durability. The consequences of electrode dilation are far-reaching and can cause a propagation of microstructural defects that compromise the mechanical integrity and function of the cell. For instance, electrode dilation can reduce the flexibility of the electrode binder during prolonged cycling, which leads to active material particles cracking and pulverizing. Irreversible dilation can also reduce the cycle life of LiBs.[37–39] In LiBs, solid electrolyte interphase (SEI) formation and the electrochemically driven growth of passivation layers on metal surfaces are a subject of dilatometric studies. ECD is sensitive to amorphous phases and SEI formation as long as there is a sufficiently large change in electrode thickness.[40] Commonly adopted LiB electrodes can undergo fragmentation and deleterious thickness changes after prolonged periods of intercalation/deintercalation, particularly at high cycling rates.[41,42] Thickness variations during charging are a confounding problem in next generation anode materials for LiBs, particularly for alloying type electrodes.

2.1.2. Graphite

Numerous carbon materials such as graphite, petroleum coke, carbon black, carbon fibre, and amorphous carbon, with a high diversity of physical and chemical features have been studied as Li ion-intercalation electrodes.[43–45] However, graphite is the most widely used commercial anode material in LiBs because of its high coulombic efficiency and cycle performance. In graphite, Li-ion occupation sites are between two adjacent C layer planes, where one Li ion is associated with a hexagonal C ring in the LiC_6 structure.[46] To date, much research effort has been focused on the chemical processing and electrochemical properties of Li-intercalated graphite which has a capability of intercalating Li to $x = 1$ in Li_xC_6, equal to a gravimetric specific capacity of 372 mAh g^{-1}.[47,48]

Dilation and contraction are common for crystals that have a layered lattice and undergo intercalation/deintercalation of guest ions. In graphite/Li cells, during discharging (applying a constant negative current) Li ions intercalate between the graphene layers and the electrode increases in height (dilates) whereas during charging (constant positive current), Li ions deintercalate causing the electrode's height to decrease (contract). Note that the notation of charge and discharge here is applicable to the graphite/Li 'half-cell' and will be different for full cells.[33]

Biberacher et al. and Besenhard et al. were among the first studies in literature to use dilatometry to investigate graphite's dilation during cycling.[49–52] Hahn et al. demonstrated that graphite electrodes undergo height changes as the stoichiom-

etry of graphite changes with Li intercalation across a time frame of 40 hours using the in-house construction described in earlier works by Hahn et al.[53] When graphite was fully intercalated and thus the height change was largest, the highest recorded value of expansion was also recorded from the dilatometer. They showed that stoichiometric changes that occur to an electrode material due to Li intercalation can be evidenced using dilatometry and the results confirmed with X-ray diffraction (XRD) studies.[54] Another example of a study that used XRD in tandem with dilatometry is Hantel et al.[55] who used in-situ XRD and in-situ dilatometry to reveal electrochemical activation of partially reduced graphite oxide (GOpr) to irreversibly modify the interlayer distance. In this case, a three electrode cell developed in-house was used for dilatometric characterisation, also used by Hahn et al. in Ref. [28] (see Figure 2a). The irreversible formation of a stable SEI layer can be accelerated by electrolyte additives, which contributes to electrode swelling.[34] An example of a commonly used electrolyte additive in LiBs is vinylene carbonate (VC). Ivanov et al. investigated how varying the concentration of VC in electrolytes affected the volumetric expansion of graphite composite electrodes in LiBs (Figure 4).

In this study, a graphite electrode with no VC additive underwent a maximum of 8 µm dilation at the end of first discharge. In contrast, a graphite electrode with 4% VC underwent a maximum of 6 µm dilation at the end of first discharge. It was concluded that irreversible dilation is largely influenced by the VC concentration in the electrode. The addition of additives allowed for a thicker SEI layer to be established which contributed to the irreversible dilation recorded. However, SEI layers are typically expected to be on the nanometre scale, and an overall decrease in irreversible dilation was observed when adding higher concentrations of VC, despite a thicker SEI layer. This was associated with differences in electrolyte decomposition and adsorption/incorporation of chemical products produced during cycling. Additional irreversible volume expansion occurred due to the incorporation of soluble decomposition products into the electrode when no additives were used.[34]

Most dilatometric studies of graphite in literature use similar variants of galvanostatic cycling parameters to record the dilation/contraction arising from continuous intercalation of Li ions. However, Bauer et al. elected to use galvanostatic intermittent titration techniques (GITT) for high rate dilatometry experiments, focussing particularly on the relaxation phenomena that graphite/nickel manganese cobalt (NMC) pouch cells underwent after current pulses.[31] They used the ECD-1 dilatometer for single electrode experiments and an in-house developed dilatometer for whole cell dilation experiments. The in-house developed dilatometer was used for high rate dilatometry experiments, and the ECD-1 dilatometer was used for low-rate dilatometry experiments. It was possible that the ECD-1 dilatometer was not suitable for fast C-rate experiments due to the large borosilicate glass separator used in the instrument, which could have contributed to diffusion limitations of Li$^+$ at high C-rates.
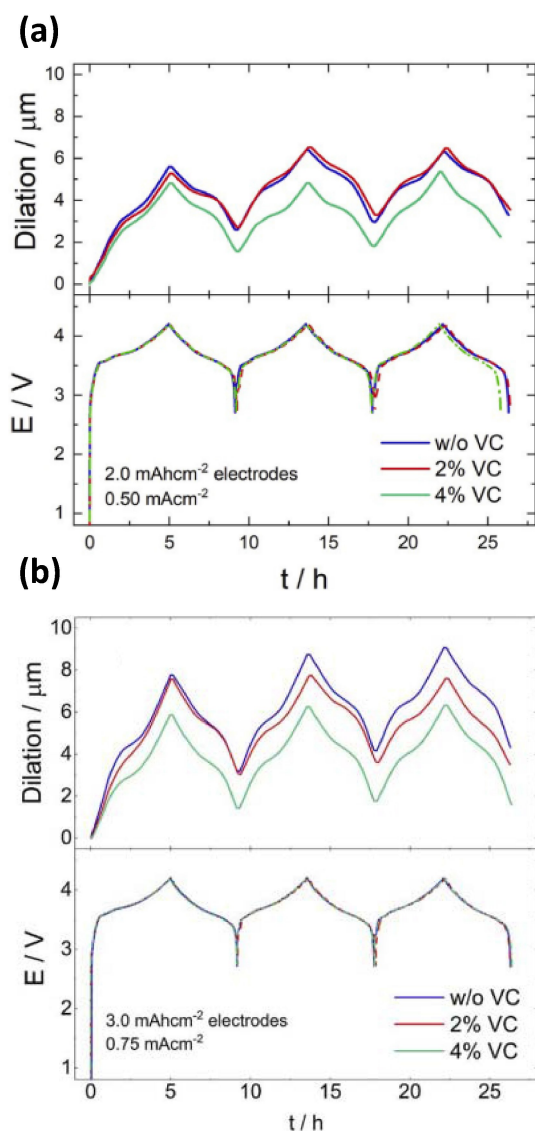
Batteries & Supercaps

Reviews
doi.org/10.1002/batt.202100027

**Chemistry
Europe**
European Chemical
Societies Publishing

(a)

(b)

Figure 4. Dilation-time (top) and potential-time profile (bottom) of Graphite/NMC cells for a) 2.0 and b) 3.0 mA h cm^{-2} nominal capacity and constant 23% porosity. ECD measurements are taken during three C/4 charge/discharge cycles. Electrolyte composition: 1 M LiPF$_6$ in EC: EMC 3:7 (w:w), without VC – (blue), 2% VC – (red) and 4% VC – (green). Reproduced from Ref. [34] with permission. Copyright (2020) Elsevier.

A total crystallographic volume expansion of 13.2% occurs when C$_6$ is fully lithiated to a composition of LiC$_6$ as confirmed using XRD.[56] However, numerous articles report the volume changes in graphite electrodes during cycling, using in-situ dilatometry, with dimensional changes ranging between 4–13% owing to differences in electrode composition, electrolyte and cell configuration.[31,46,47,56–64] Graphite particles can rearrange themselves in the particle-binder matrix as they expand and contract during cycling, which leads to severe contact stresses and fracturing of particles that are packed closely together.[65] Electrode delamination that causes the graphite particles to no longer be connected to the current collector has also been proposed as a degradation mechanism that influences ECD measurements.[33] In addition, calendering

during the manufacturing process can give rise to stresses at the cell level, which causes the electrode material to fracture.[66] Nonetheless, despite variation in the scale of thickness change, a consistent dilation/contraction behaviour has been recorded across numerous reports, reconciling the thickness changes that occur during phase transitions at certain voltages.

2.1.3. Silicon

Silicon (Si) is the leading candidate anode material to replace graphite, as it has a theoretical specific capacity of ~4200 mA h g^{-1} when alloyed with Li as Li$_{22}$Si$_5$.[67,68] Crystalline Si is electrochemically lithiated to form amorphous Si via a two-phase mechanism.[69,70] The two phase mechanistic behaviour is likely due to the large activation energy necessary to break up the crystalline Si matrix: a high concentration of Li atoms near the reaction front is required to weaken the Si–Si bonds, resulting in favourable lithiation kinetics and the observed two phase behaviour.[71] The amorphous phase that forms at the expense of the crystalline Si is highly lithiated ($x = 3.4 \pm 0.2$ Li atoms per Si atom close to the stoichiometry of the common terminal crystalline phase at room temperature, where $x = 3.75$).[72] Highly lithiated Si formation at the reaction front leads to significant volume expansion of up to 270%–300%, which in turn causes large gradients in transformation strain.[73–75] Expansion issues related to charging Si remain the largest obstacle to overcome for Si anodes in commercial application.[76–79]

Dilatometry has been used in studies to understand the thickness change of carbon, SiO, Si and SiN electrodes.[32,80–87] Yu et al. showed that prolonged cycling of Si electrodes with active particles on the micro-scale leads to intrinsic volume expansion, and that particles vertically rearrange themselves during charge/discharge.[88] They highlighted that, as particles swell to fill empty voids, there is a hysteresis in the thickness changes recorded (changes occur undetected by the dilatometer). It is only when the particles are displaced vertically away from the electrode that height changes were detected. This demonstrates the importance of corroborating dilatometry with other techniques that can provide information on morphological changes on the particle or fibre scale as some mechanical phenomena may go undetected.

It is noteworthy that some studies have coupled dilatometry with acoustic measurements to provide more granular information on single electrode and full-cell volume changes. Tranchot et al. coupled with acoustic emission (AE) measurements and scanning electron microscopy (SEM), to study the effect that Si particle size (85 nm *versus* 230 nm) has on the mechanical stability of composite Si/C/carboxymethyl cellulose (CMC) binder electrodes.[89] It was demonstrated that operando dilatometry coupled with AE experiments and post-mortem SEM observations gives valuable quantitative information about the morphological degradation of Si-based electrodes. In the case of smaller particles, the larger specific surface area means there is insufficient CMC binder to prevent film delamination and maintain a conductive network between the electrode

Batteries & Supercaps

Reviews
doi.org/10.1002/batt.202100027

Chemistry Europe
European Chemical
Societies Publishing

components during expansion/contraction of the Si electrode. Tranchot et al. proposed that electrode degradation is mostly determined by the cohesive/adhesive properties of the electrode, as opposed to the cracking resistance of individual Si particles.[89]

Implementing a high-modulus polyimide (PI) layer is common when using micron-sized Si electrodes to enhance the adherence of particles with the coating, and to prevent delamination of active particles from the electrode when Si undergoes significant volume expansion. For example, Lee et al. suppressed volume expansion in Si electrodes by electrospraying a PI layer onto a thin-film Si electrode. The dilatometer can be used to calculate the volumetric capacity (Q_{vol}) using the following equation [Eq. (1)]:

$$Q_{vol} = \frac{Q_{areal}}{\text{Electrode thickness}} \qquad (1)$$

Where Q_{areal} is the areal lithiation capacity (mA h cm^{-2}) of the electrode and the electrode thickness is obtained from in-situ dilatometry.

Lee et al. found that the PI layer coated electrode expanded less than a Si thin film electrode that did not have a PI layer. It was concluded that the PI layer maintained the electrode's integrity and prevented electrode delamination and material pulverization during cell cycling.[90] The use of a PI coating on high capacity anode materials such as antimony is discussed in the next section. However, at the time of this review, there is limited dilatometric research of the effectiveness of these PI coatings when used with electrodes composed of higher capacity anode materials for LiBs such as Sb and Sn.[91]

Whilst it is important to compare electrodes of different elemental composition, it is also necessary to account for how particle dimensions in an electrode can impact the rate of capacity fade and influence thickness variations.[92,93] It is widely reported that nano-sized Si particles can accommodate the stress build-up during lithiation and delithiation, and voids among the particles can also absorb some of the volume changes.[94,95] However, nano-sized Si particles are difficult to handle and can be energy intensive to produce. Tan et al. investigated thickness variation of micron sized SiO particles using dilatometry (Figure 5). They used a PI coating system to reduce thickness changes during cycling with the intention to prevent rapid capacity fade that would otherwise be observed for micron sized SiO particles with no protective coating system.[91]

The SiO electrodes underwent significantly higher thickness changes than the SiO electrodes that had a self-assembled monolayer (SAM) and PI, suggesting that the SAM/PI coating helps to maintain the mechanical integrity of the particles and electrode during cycling. The authors propose that an enhanced PI coating with a SAM can be applied to various alloy-based and conversion-based anode materials for LIBs to suppress electrode degradation.[91]

Section 2.1.2 reviewed examples of varied conductive additives in graphite electrodes to assess how additives affect electrode volume changes during cycling. Different conductive
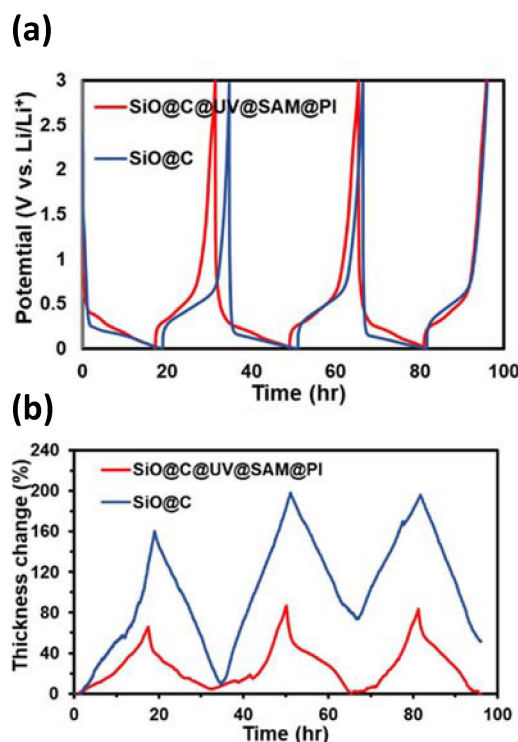
(a)

(b)

Figure 5. a) Potential-time profile and thickness change-time profile for a carbon-coated SiO (SiO@C) electrode and b) a carbon-coated SiO electrode with a self-assembled monolayer and PI surface layer that was UV treated (SiO@C@UV@SAM@PI), tested at 150 mA g^{-1} with an in-situ dilatometer. Reproduced from Ref. [91] with permission. Copyright (2020) Elsevier.

additives have also been used in Si-based electrodes. For instance, Karkar et al. prepared Si electrodes with either carbon black, carbon nanofibers or carbon nanoplatelets (conductive additives) and investigated the associated volume changes with each electrode using the ECD-2 dilatometer.[96] They found that deleterious volume changes of Si electrodes occur above a critical silicon mass loading for which high mechanical stresses are unavoidable. This critical Si mass loading depends on the conductive additive used in the electrode mixture. Carbon nanoplatelets were found to be the most ideal additives as they operate as a lubricant, allowing the sliding of Si particles as they dilate/contract. This is suggested to avoid mechanical stresses and limit the rupture of SEI. Dilatometry findings showed carbon black-containing electrodes to have the largest thickness changes during cycling, suggesting that carbon black is the least effective conductive additive. The electrode's conductive network was unable to be maintained during drastic Si volume changes.

Calendering is a commonly used compaction technique for LiB electrodes; it has a significant impact on porosity and thus the electrochemical performance of LiBs.[97–100] Calendering involves pressing an electrode and subsequently increasing its volumetric energy density. It is performed after the electrode casting and drying steps, and alters numerous physical properties such as the lithium diffusion pathway length, the electrode porosity and interparticle contact,[101] and can also be a cause of non-electrochemically driven particle cracking.[102] Dilatome-

Batteries & Supercaps

Reviews
doi.org/10.1002/batt.202100027

Chemistry Europe
European Chemical
Societies Publishing

try can be used to compare and contrast volume changes in calendered and non-calendered electrodes to assess the impact of calendering on the electrode's dimensional changes. The direction of electrode dilation occurs mainly parallel with the direction of calendering, which is perpendicular to the current collector.[103] Karkar et al. demonstrated an improved cycle life and reduced thickness change in calendered Si-based electrodes using operando dilatometry.[74]

During prolonged cycling, the electrode binder can undergo significant strain due to continuous dilation and expansion.[104] However, studies have found that crosslinked binders have the potential to enhance Li ion diffusion and reduce the strain undergone by the electrode over time.[105,106] Gendensuren et al. investigated Si electrodes and found that a dual-crosslinked binder was helpful in minimising volume expansion. They stated that the self-healing attribute of crosslinked poly(acrylamide) (PAAm) may have been responsible for minimising volume expansion.[106] In addition, Jeong et al.[32] showed that the pore forming agent Poly(methyl methacrylate) (PMMA) has the ability to 'unzip', reducing volume expansion by forming pores in Si-based composite electrodes, resulting in little deformation during lithiation. Unzipping refers to the depolymerization of specific polymers to monomers. On the other hand, untreated Si electrodes used as a control showed severe and continual increase in dilation with cycling.

Binders play a crucial role in maintaining the mechanical integrity of electrodes during prolonged cycling and can be readily tailored to specific active materials and applications. Jackel et al. investigated the dimensional changes of battery electrodes containing either a stiff or soft polymeric binder using dilatometry.[107] They suggest that the optimal polymeric binder should neither be completely rigid nor too soft to enable unrestricted electrode volume change and prevent the binder from viscously creeping into the active material. Binder properties are highly sensitive to changes in temperature. While Jackel et al. kept temperature constant to compare either stiff or soft polymeric binders, Park et al. explored the impact of thermally treating a Si–Ti–Fe–Al alloy electrode with a poly amide-imide (PAI) binder. The volume expansion of the electrode is investigated at three different temperatures: 200 °C, 300 °C and 400 °C, respectively. After full lithiation (discharge), the Si electrode treated at 200 °C expanded by up to 531%, whereas the Si electrode at 300 °C and 400 °C showed thickness changes of 312% and 436%, respectively. The Si alloy electrodes that were heat-treated to greater than 300 °C showed less thickness change during lithiation/delithiation. Such changes were attributed to enhanced mechanical strength of the PAI binder at elevated temperatures.[108] Yang et al.[109] also report that heat treating PAI binders can improve the cycle performance of Si-alloy electrodes that contain PAI binder. They attributed the enhanced capacity retention of Si electrodes to the improved mechanical strength of PAI binders caused by the rearrangement of molecular chains at elevated temperatures. Other than thermal treatment, the mechanical strength of binders can be enhanced using chemical etching. Metal-assisted chemical etching is a surface modification technique that is used to enhance capacity retention and has

become attractive for modifying the surface of silicon based on galvanic displacement.[110] Kim et al. investigated the effect of a binder on Si nanostructure electrodes that were etched using silver. The poly-vinylidene difluoride (PVdF) and PI binders were evaluated on the basis of electrochemical and ECD measurements.[111] There were minimal differences in thickness change between the Si-PVdF and the etched Si-PVdF electrodes; however, the etched Si-PI electrode showed significantly less thickness changes than the other two tested electrodes during cycling. Therefore, the PI binder played a pivotal part in suppressing the physical thickness changes observed during insertion and extraction of Li ions. The findings suggest that PI binders enable the electrode to better maintain an electric conduction network which would theoretically improve LiB durability during prolonged cycling.

Kim et al. demonstrated that dilatometry can be used to provide information about the role of reduced graphene oxide (RGO) in Si composite anodes. RGOs were used in Si/carbon nanotubes (CNT) and Fe_2O_3/carbon-nanofiber (CNF) during galvanostatic cycling in order to accommodate volume expansion. The RGO buffering agent had a porous framework with a flexible texture due to the lack of rigid connections between adjacent nanosheets. ECD revealed an overall change in electrode thickness of 11% for the Si/carbon-nanotube (CNT) and Fe_2O_3/carbon-nanofiber (CNF) anode-material electrodes. This was smaller than expected for such oxide-based electrode materials and is presumably because the RGO played a buffering role in the Fe_3O_4/RGO volume changes during the Fe_3O_4–Li ion reactions, resulting in the delayed and gradual Fe_3O_4/RGO volume expansion. The composite electrodes also exhibited excellent cycling stability.[112]

Extensive dilatometric research has been carried out on Si-based electrodes for LiBs (see Table 1 and Figure 6). The experiments can vary between investigating different electrode compositions, different electrolytes of varied concentrations, the effect of using different binders/coatings, conductive
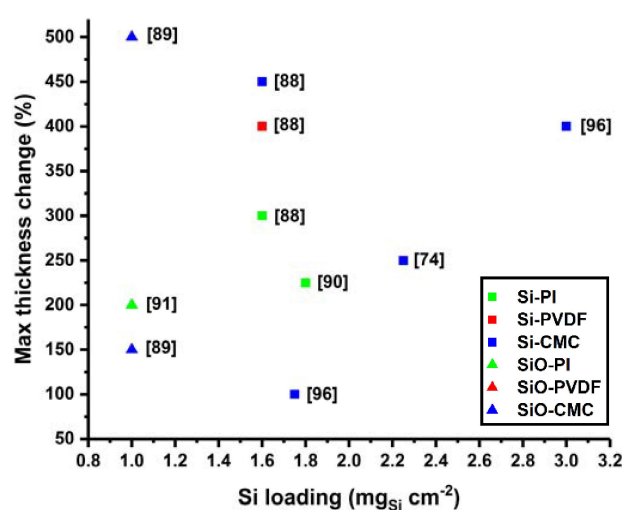

Figure 6. The maximum thickness change (%) recorded for different Si electrode compositions with varying Si loading from works discussed in section 2.1.3. Each point is labelled with the appropriate citation.

Batteries & Supercaps

Reviews
doi.org/10.1002/batt.202100027

Chemistry Europe
European Chemical
Societies Publishing

Table 1. Maximum thickness change recorded for different silicon electrode compositions discussed in Section 2.1.3.

Active material	Si loading [$mg_{si}\,cm^{-2}$]	Binder/coating	Conductive additive	Composition ratio (AM/Binder/CA)	Max thickness change [%]	Ref.
Si	1.6	PVdF	Acetylene black	60/20/20	400	[88]
Si	1.6	CMC	Acetylene black	60/20/20	450	[88]
Si	1.6	PI	Acetylene black	60/20/20	300	[88]
Si	1.8	PI	N/A	90/10	225	[90]
Si	~3	CMC	Graphene sheets (GM15)	80/08/12	400	[96]
Si	~1.75	CMC	Carbon black	80/08/12	100	[96]
Si	2.25	CMC	Graphene sheets (GM15)	80/08/12	250	[74]
SiO	1.0–1.1	PI	Carbon black	60/10/20	200	[91]
SiO (2.1 % O)	1.0 ± 0.1	CMC	Carbon black	73.5/14.5/12	500	[89]
SiO (1.29 % O)	1.0 ± 0.1	CMC	Carbon black	73.5/14.5/12	150	[89]

additives and the installation of pore forming agents in the electrode composition. Numerous studies using Si-based micro-particles with an inactive matrix to accommodate volume expansion have been published.[113] Furthermore, various electrochemical in-situ techniques can be used in conjunction with ECD to provide more information on the lithiation mechanism in Si electrodes such as X-ray diffraction,[114] Raman spectroscopy,[115] solid-state NMR[81] and differential electrochemical mass spectrometry (DEMS).[80]

2.1.4. Other High-Capacity Anode Materials

There are numerous high-capacity anode materials that have the potential to supersede anodes currently used in commercial LiBs. Alternative anode materials have been explored to meet the increasing demand of batteries with higher energy density.[116,117] However, electrode cracking seriously hinders their application.[118,119] Nano-sizing is a commonly adopted method to reduce fracturing of individual particles, but capacity fading still occurs owing to large volume change and loss of contact in the electrode during Li insertion and extraction. A strategy was devised by Li et al. to reduce cracking formation between particles in a SnO_2 electrode by constructing a crack resistant high-modulus PI coating.[120] Electrode thickness changes during galvanostatic cycling suggested that cracking and expansion of the electrodes reduced, which was attributed to the PI coating exerting a compressive force that kept particles together. Li et al. concluded that this method of suppressing volume expansion could be applied to various electrode compositions that are highly susceptible to large dimensional changes to aid development of anodes for LiBs.[120]

High-capacity anode materials such as antimony are promising because their operating voltage is approximately 0.8 V vs Li, far from the Li plating potential (though this does of course reduce the operating cell voltage). However, Sb electrodes also undergo drastic volume expansion during cycling which has a crippling effect on the cycle life of the cell and capacity retention.[121] The theoretical volume expansion of Sb-based electrodes lies between 121 and 132%.[122] Wang et al. explored the integration of a PI and CMC binder into the electrode's slurry composition to suppress particle cracking and hold the particle together, enabling Sb anodes to utilize micron sized particles during high C-rate protocols.[123] Thickness

changes of the PI treated electrodes were measured using Sb electrodes with 9.4% wt. PI showed lower thickness changes than electrodes with 4.7% wt. PI in the electrode composition. The results suggest that volume change was reduced with PI-cellulose interaction. The PI binder reduced pulverisation of particles during cycling. Particle pulverisation is one of the main obstacles to wide-scale use of high capacity anodes.

Wang et al. carried out a comparative study of incorporating a sulfur or selenium matrix into Sb-based electrodes to investigate their electrochemical performance as LiB electrodes. It was found that volume expansion was reduced for Sb_2S_3 and Sb_2Se_3 electrodes because S and Se matrixes inhibit crystallization of Li_3Sb during lithiation, enhancing the electrode's stability. In addition, this study corroborated various techniques with dilatometry, such as X-ray diffraction, Raman spectroscopy and SEM.[122] Ma et al. used dilatometry to study silver electrodes and α-MnS/S-doped C microrod composites.[124,125]

2.1.5. Cathode Chemistries

Cathode dilation is often neglected in dilatometric research because thickness variations at the cathode are of a much smaller magnitude compared to the anode, and thus the consequences of cathode dilation are thought to be far less detrimental to the cycling capability of LiBs.[31] Although studies seldom report cathode material dilation in comparison to anodic dilation, Rieger et al. reported a thickness change of 1.8% for a $LiCoO_2$ cathode during delithiation using dilatometry.[126] They reported high overpotentials in potential curves and argued that it was a result of the large distance between the reference electrode and working electrode (ca. 500 μm). Yu et al. highlighted limitations in dilatometry cell configurations, with overpotentials reported due to mass diffusion limitations.[88] In order to conduct dilatometry experiments, Rieger et al. assembled segments of the pouch cell battery electrode into a dilatometer; the battery selected had two single-sided cathode layers towards the top and bottom of the electrode stack, which were used for the dilatometric experiments of the cathode (symmetrical cell). For the dilatometric experiments on the graphite anode, an electrode was cut and placed inside the dilatometer from the pouch cell electrode bilayer. Although graphite was coated on both sides of the bilayer, only one side participates in the electrochemical

Batteries & Supercaps

Reviews
doi.org/10.1002/batt.202100027

Chemistry
Europe
European Chemical
Societies Publishing

reaction inside the dilatometer assembly. This is because the copper current collector acts as a barrier for Li-ions. This study demonstrates that dilatometry can be a useful tool for investigating commercially available Li-ion batteries with a pouch cell configuration. The drawback to this approach is that it destroys the pouch cell because it cannot be reassembled after measurements.

NMC is a cathode material widely used in commercial LiBs. The stoichiometry and thus structure of NMC can vary depending on the ratio of nickel, manganese and cobalt, respectively.[127] Nayak et al. demonstrated that dilatometry can be utilised to monitor reversible and irreversible processes of NMC in LiBs. They prepared a Li rich $Li_{1.17}Ni_{0.20}Mn_{0.53}Co_{0.10}O_2$ cathode material using a sol-gel method and investigated the dimensional changes that occur during galvanostatic cycling (see Figure 7).[128]

In-situ ECD revealed an irreversible contraction/expansion during charge/discharge and correlated this phenomenon to irreversible capacity loss during the first cycle. A large voltage hysteresis and substantial voltage loss on first charge/discharge is thought to occur because of the formation of molecular O_2 at 4.6 V versus Li^+/Li which becomes trapped in voids within the particles in the bulk and also lost from the surface. The O_2 that forms during first charge causes the disorder of the transition metal ions associated with the loss of the honeycomb structure, which thus forms vacancy clusters that accommodate O_2.[129] Dilatometry confirmed that reversible electrode contraction/expansion occurred after initial cycling, quantitatively confirming the good cycling stability of this material. The absolute change in electrode thickness during cycling was about 0.27 μm during prolonged cycling. The electrode periodically "breathed" with each cycle by less than one percent compared to its total thickness. Overall, the dilatometer proved to be a very useful instrument in examining the reversible and irreversible processes in composite electrodes with thickness changes as small as 1% of the total electrode thickness. The dilatometer contained a high-resolution capacitive transducer that can detect dimensional changes at the WE down to a few res resolution. Dilatometers with a different detector have also been used. Ariyoshi et al.[130] used a dilatometer with a linear voltage displacement transducer to detect the dimensional changes of $LTO/LiCoMnO_4$ LiB during galvanostatic cycling. The same model was used by Nagayama et al. and is an in-house fabricated assembly.[131] The dilatometer uses a pouch cell test sample and thickness changes of the cell are transmitted via a spindle to a linear voltage displacement transducer. The transducer is connected to an amplifier that converts displacement signals in micrometres to a voltage signal in mV.[131]

There has been renewed interest in vanadium oxide as a cathode material in LiBs. Layered vanadium oxides are promising cathode materials owing to their low cost, high capacity and moderate voltage.[132,133] Barker et al. assembled an in-house dilatometer with a linear voltage displacement transducer to measure the thickness changes of an entire LiB pouch cell with a vanadium oxide (V_6O_{13}) and lithium metal electrode.[134] During lithium insertion into the V_6O_{13} and Li^+
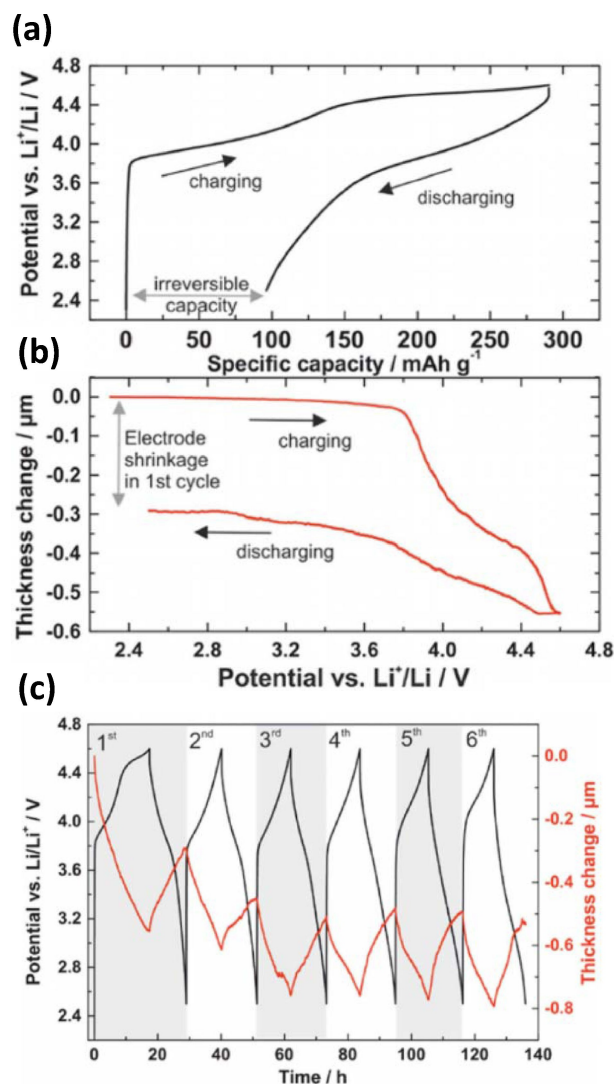
(a)

(b)

(c)

Figure 7. a) Potential-capacity profile and b) thickness change-potential profile of $Li_{1.17}Ni_{0.20}Mn_{0.53}Co_{0.10}O_2$ at 20 mA g^{-1} (C/10 rate) in the potential range of 2.5–4.6 V in 1 M LiPF$_6$ in EC/DMC solution. The potential-time and thickness change profile is shown in (c) for $Li_{1.17}Ni_{0.20}Mn_{0.53}Co_{0.10}O_2$ at 20 mA g^{-1} (C/10 rate) in the same voltage range as (a) and (b) for six consecutive cycles. These images were reproduced from Ref. [128] with permission. Copyright (2019) Wiley-VCH.

dissolution from the anode there was a gradual decrease in the overall cell thickness. The converse was observed during Li extraction from V_6O_{13} and Li plating onto the Li metal. Nonetheless, the thickness changes were seen to be highly reversible over the voltage range used. The thickness increases in V_6O_{13} corresponded to around a 1.7% change in the electrode's initial thickness. The volume fraction of the V_6O_{13} in the composite electrode material was approximately 0.27. The thickness changes were found to be in accordance with the literature reported unit cell expansion/contraction of V_6O_{13} cathodes, caused by lithium insertion/extraction.[134–136]

Cathode materials also undergo volume changes during cycling which are dependent on their stoichiometry and structure. Nonetheless, the influence that cathode material dilation and contraction has on battery performance, and

Batteries & Supercaps

Reviews
doi.org/10.1002/batt.202100027

Chemistry Europe
European Chemical
Societies Publishing

overall cell dilation, is often neglected as it is assumed to be an order of magnitude smaller than the anode dilation.[31] In fact, multiple studies that report dimensional changes of cathode material primarily focus on pouch cells as opposed to individual electrodes.[137,138] It is possible that dilatometric investigations focusing entirely on cathode materials are rarer compared to their anode counterpart owing to the finer resolution required to notice small details in thickness changes of cathodes. The dilatometry instruments that currently exist may not be capable of detecting the finer details that would explain the thickness changes of the cathode which could be associated with crystallographic changes.

2.2. Dilatometric Characterisation of NiBs

It is imperative to investigate the influence of the electrolyte on sodium ion intercalation in NiB electrodes given that it is widely reported that solvents can influence co-intercalation reactions and volume changes of the electrode.[139,140] Goktas et al. investigated the reversible process of solvating Na ions into a graphite electrode from ether electrolytes (see Figure 8). The electrode was found to periodically breathe by about 70–100% during cycling.[141]

Despite the large volume changes undergone by the graphite electrodes during sodiation/desodiation, this process was not found to hinder reaction reversibility. It is proposed

Figure 8. In situ dilatometry measurements for the first five cycles at C/10 of the graphite electrode in ether electrolyte. This figure was reproduced from Ref. [141] with permission. Copyright (2018) Wiley-VCH.

that this could be a result of two possibilities: firstly, no SEI is formed in an ether solvent, or an SEI reversibly forms and breaks, dissolving into the ether electrolyte with each cycle, due to large volume expansions. Karimi et al. set out to build on the work of Goktas et al. by studying the volume changes of a graphite electrode in ether electrolytes of varied chain lengths.[142] Graphite electrodes underwent highest expansion during the first sodiation in all ether electrolytes (100–130% of initial thickness), possibly due to initial SEI formation. The graphite electrodes followed with an overall decrease in thickness during consecutive cycles as was found by Goktas et al. The overall decrease in electrode thickness suggests an electrode rearrangement in ether solvent during prolonged cycling.

The two most commonly used binders in LiBs and NiBs are PVDF and CMC, each with different mechanical properties.[143] Escher et al. monitored the effect of varying the type of binder on volumetric expansion of graphite electrodes in NiBs using in-situ ECD.[143] They found that using CMC instead of PVDF was effective in reducing the electrode expansion during initial sodiation. However, during cycling, the electrode breathing for both binders was comparable. They then added ethylenedi-amine (EN) as a co-solvent to the electrode compositions and found that this addition strongly reduced the electrode expansion during initial sodiation (175% without EN reduced to 100% on addition of EN) as well as breathing of the electrodes that followed. The authors suggest that solvent co-intercalation led to pillaring of the graphite lattice and that the addition of EN to the electrode composition caused a change in the sodium storage mechanism. An alternative carbonaceous anode to graphite for NiBs is hard carbon. Alptekin et al. used dilatometry to monitor thickness variation of electrodes composed of hard carbon and CMC binder.[144] There are noticeable similarities to the dilation profiles of graphite electrodes by Escher et al. such as highest expansion occurring during the first sodiation cycle and differences between the initial thickness of the electrode and desodiated state.[141,143] The dilation profile of hard carbons also have an initial sloping region, a plateau and final sloping region during sodiation which follow a similar dilation profile to graphite electrodes in Lithium ion chemistries that are discussed previously in this review.[33,34,54] This finding suggests that carbon-based electro-des may have similar dilation profiles in different metal ion chemistries despite having different charge-storage mecha-nisms.

As with LiBs, alternative anode candidates that can super-sede graphite with higher theoretical capacities in NiBs include Na_3P, $Na_{15}Sn_4$, Na_3Sb and crystalline germanium. However, electrode materials such as germanium undergo larger volume changes than graphite resulting in severe capacity fading.[145–148] The electrode strain corresponding to sodiation/desodiation in crystalline nanoporous Ge-based anodes was monitored by Li et al.[18] Volume expansion was highlighted as the primary cause of capacity fading in Ge-based anodes. It was proposed that electrodes that undergo stable reversible volume changes during cycling may be required to overcome capacity fade as opposed to electrodes that undergo minimal irreversible
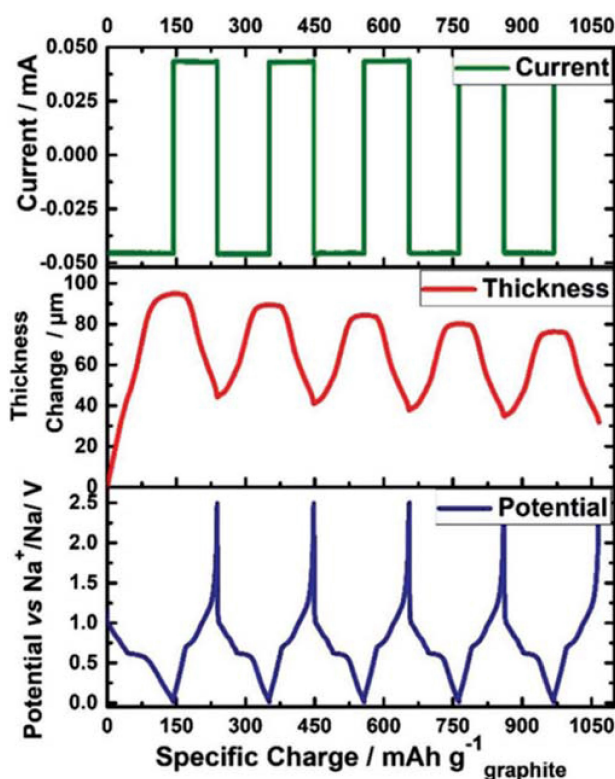
Batteries & Supercaps

Reviews
doi.org/10.1002/batt.202100027

Chemistry Europe
European Chemical
Societies Publishing

volume change. In addition, Brehm et al. measured a reduced "breathing" effect observed for tin-antimony anodes during galvanostatic cycling, by optimising ball-milling time during synthesis.[149] Numerous dilatometric studies of NiBs investigate variations of tin electrodes. Studies have examined anodes composed of tin with other metals, and the effect of using different electrolyte solutions. The sodiation/desodiation mechanism in tin electrodes has been studied in carbonate-based electrolytes and glyme based electrolytes to demonstrate how SEI formation is effected by the electrolyte used.[150] Tin and phosphorus stand out as promising cathode materials for NiBs given their large theoretical capacities (847 mAh g^{-1} and 2596 mAh g^{-1} for Sn a P, respectively) and their suitably low operating voltages (0.25 and 0.6 V vs. Na/Na$^+$ for Sn and P respectively). Unfortunately, their drawback is that they suffer severe capacity decay during cycling. Wang et al. investigated a combination of Sn and P to determine if a SnP$_3$ anode composition can lead to an improvement in electrochemical performance.[151] However, Sn agglomerated in the pristine SnP$_3$ anode upon cycling causing significant capacity fading. The capacity fading was initially ascribed to the volume expansion of ca. 430% at the SnP$_3$ anode, far larger than the 60% electrode thickness increase of Sn when using 1 M NaPF$_6$-DME electrolyte. However, they found that significant volume expansion of the anode did not always correlate with capacity fading. They concluded that these thickness variations are primarily caused by the alloying mechanism of the SnP$_3$ anode, rather than Sn agglomeration during cycling. Sn and P alloys with Na to form alloy phases Na$_{3.75}$Sn and Na$_3$P, respectively, inevitably with an accompanying large volume expansion of the host material. In the case of Sn electrodes, only alloys of Na with Sn form so less detrimental volume increases should be expected as no P is present.

NiBs are expected to generally undergo larger thickness variations during charge/discharge cycles because sodium ions are larger than lithium ions. In fact, Brehm et al. compared Cu$_3$P as an anode material for NiBs and LiBs and larger volume expansions were recorded for Cu$_3$P in sodium half cells compared to lithium half cells owing to larger sodium ions during discharge (261% for Na compared to 190% for Li). In addition, diglyme solvents were compared to carbonate solvents in both Li and Na half cells. More stable "breathing" was recorded when the diglyme electrolyte was used as a solvent and a rapid degradation was found for carbonate electrolytes. An unfavourable SEI formation is thought to occur when using carbonate electrolytes because larger expansion/contraction was recorded during the initial discharge cycles in both Li and Na half-cell chemistries, indicative of more side reactions occurring.[40] Severe side reactions and less stable SEI formation lead to rapid capacity fading.

Palaniselvam et al.[152] identified a change in sodium storage mechanism from co-intercalation to insertion when ball milling graphite into graphite nanoplatelets (GnP). The effect that a change in sodium storage mechanism has on thickness variation can be profound. Dilatometry showed that a change in electrode thickness for nitrogen-doped tin treated graphite nanoplatelets (SnNGnP) during cycling was just 14% and

therefore much smaller compared to what one would expect from the 420% that arises from conventional Na$_{3.75}$Sn. This is direct evidence of the carbon matrix effectively buffering the volume change of the Sn during cycling. The porous structure of the nanocomposite had sufficient free space to accommodate expansion. The small change in electrode thickness is likely the key factor enabling the excellent cycle life. The loose and open structure of the nanocomposite allowed for tin to expand within the electrode. Huge electrode expansion that would otherwise contribute to electrode degradation is effectively mitigated. Palaniselvam et al.[153] further investigated Sn-based electrodes in NiBs. In this study, graphite and tin-graphite composite electrodes were found to have distinctly different dilation profiles during cycling, owing to the alloying reaction of Na with Sn. A combined storage mechanism based on graphite intercalation formation and Na–Sn alloy formation were measured using in situ ECD and in situ XRD. Whilst the theoretical volume expansion for Sn is 420% only 3% was due to Sn during the first cycles of Sn-graphite which was most likely due to the good dispersion of Sn nanoparticles in the graphite matrix. This work could be expanded by using a lithium-based electrolyte to explore how these electrode materials fare with a lithium half-cell chemistry with in-situ ECD and in situ XRD.

Finally, Palaniselvam et al. explored how treating Sn$_4$P$_3$ electrodes with nitrogen-doped hard carbon (NHC) influences thickness variations during cycling compared to Sn$_4$P$_3$ and "Sn$_4$P$_3$"/NHC electrodes. For the Sn$_4$P$_3$ electrode, the effective thickness change was in the range of 11–16.8 μm, which corresponded to an increase of about ≈53%. Cycling of Sn$_4$P$_3$ was hardly possible and rapid degradation was observed. For the "Sn$_4$P$_3$"/NHC electrode, the average thickness change of the electrode was around 4 μm, i.e., the electrode expanded around 12% during sodiation. The use of NHC reduced the relative expansion of Sn$_4$P$_3$ electrodes and improved cycle life, leading to a fairly reversible stability during cycling.[154]

2.3. Dilatometric Characterisation of Li Solid-State Batteries (SSBs)

2.3.1. Dilatometry During Processing

Numerous dilatometry studies focus on the dimensional changes that occur in SSB electrolyte materials during processing.[155–158] Processes that can cause dimensional changes in SSBs include sintering, densification and contraction. Sintering is a critical processing technique in the production of ceramic electrolyte materials that uses high temperatures to compact ceramic powders into a solid form. Reducing the porosity and increasing the density -i.e. densification - of ceramics improves their mechanical properties. A dilatometer can be used to measure the contraction of different ceramic powders during densification and use this as a reflection of how well the ceramic powders were sintered and the effectiveness of using certain sintering aids. Sintering aids are well established in processing to help reduce sintering

Batteries & Supercaps

Reviews
doi.org/10.1002/batt.202100027

Chemistry Europe
European Chemical
Societies Publishing

temperature and still achieve acceptable densities of SSB pellets.

As previously alluded to in section 1.2, the high temperature ranges used in SSB processing make the push rod dilatometer (see Figure 9) the instrument of choice. Push rod dilatometers consist of an oven (furnace), push rod and a LVDT. When the sample material changes in length, the push rod (connected to the sample) transmits the changes in length of the sample material to the LVDT sensor where the absolute changes in length of the sample material are determined. Temperature curves can be realised using the oven, and thus changes in length of the sample can be determined as a function of temperature which is useful for studying SSB sintering temperatures.

Jonson et al. measured the changes in length of $Li_7La_3Zr_{1.75}Nb_{0.25}Al_{0.1}O_{12}$ (LLZNbO) solid electrolytes during densification.[155] Dilatometric analysis showed sintering of LLZNbO when using 6 wt% Li_3BO_3 (LBO) as a sintering aid at 710 °C. As the temperature was increased, shrinkage of LLZNbO pellets increased. However, the optimal LBO content for ionic conductivity in LLZO pellets sintered at 1000 °C was between 1 and 2 wt% LBO, attributed to the elimination of LBO-substrate interactions. At this LBO level, ionic conductivity in pellets was $\sim 2.5 \times 10^{-4}$ S cm^{-1} after sintering in an argon atmosphere at 1000 °C for 6 h. Shin et al. also used LBO as a sintering aid when investigating the sintering behaviour of $Li_7La_3Zr_2O_{12}$ (LLZ) solid electrolytes heated at a rate of 10 °C min^{-1} up to 1200 °C.[157,158] When LLZ was sintered without the LBO sintering aid, shrinkage occurred rapidly above 1000 °C. Whereas, LLZ heated in the presence of LBO shrunk at around 700 °C, which is much lower than the temperature required for shrinkage of pure LLZ and a similar sintering temperature reported by Jonson et al. when using the same sintering aid with LLZNbO.[155] Dilatometric measurements revealed that the shrinkage of the LLZ-8 wt% LBO composite occurred in two steps; one at 700 °C and the second above 800 °C, suggesting that the LLZ-LBO underwent two independent sintering processes. They also revealed that the density of the LLZ-8 wt% LBO composite sintered for 8 h at 1100 °C was much higher (86.4 %) than that of pure LLZ (64.0 %), achieving acceptable SSB densities at a lower sintering temperature. The shrinkage of LLZ was significantly influenced by the wetting behaviour of LBO, which started to shrink at 630 °C and started melting at 850 °C.
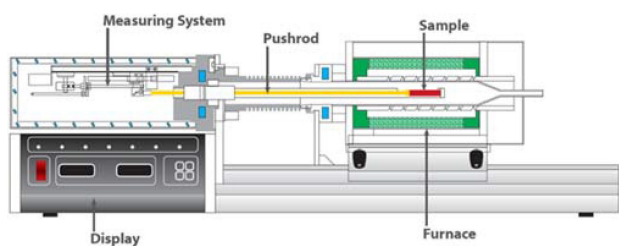

Figure 9. An illustration of the Linseis Model L75 dilatometer used by Jonson et al.[159] Image is reproduced from https://www.linseis.com/en/products/dilatometer/l75-pt-horizontal/. Copyright (2021) Linseis GmbH.

Dilatometry demonstrates that $Li_{1+x}Al_xTi_{2-x}(PO_4)_3$ (LATP) ceramic pellets with high relative density can be achieved by sintering powders in the region of 900 °C.[160] Davaasuren et al. investigated the dimensional changes of pristine LATP pellets with respect to temperature.[160] LATP pellets hardly shrank up to 650 °C, maintaining 95 % of their original thickness. However, this was followed by a sharp shrinkage during active densification. As sintering temperature increased, the diffusion rate gradually increased, promoting grain growth and reducing ceramic porosity. A dense pellet with a well-defined microstructure was recorded at 900 °C. Different stoichiometries of LBO can be used as a sintering aid in SSB electrolyte densification. Sintering in the presence of $Li_2B_4O_7$ was found to stabilise the microstructure of the LATP electrolyte by acting as an ion-conducting bridge between LATP grains, enhancing the contact between grains and strengthening the grain boundaries.

Hupfer et al. investigated the changes in length of $LiTi_2(PO_4)_3$ (LTP) and LATP pellets during densification using $LiTiOPO_4$ as a sintering aid. In this case, shrinking behaviour was monitored from 600 °C to 1200 °C. They found that by sintering LTP with $LiTiOPO_4$ the sintering temperature reduced significantly from 1200 °C to around 1050 °C. By measuring the associated shrinkage of LTP and LATP as the temperature was ramped up to 1200 °C, 900 °C was found to be a sufficient sintering temperature for the densification of LATP in the presence of $LiTiOPO_4$. In summary, dilatometric measurements have shown that $LiTiOPO_4$ and different stoichiometries of $Li_xB_yO_z$ (LBO) are effective in reducing the sintering temperature of SSB pellets and that acceptable SSB pellet densities can still be achieved, despite the reduction in temperature.

2.3.2. Dilatometry During Operation

it is also possible to use push-piston dilatometers to study SSB materials at room temperature. Zhang et al. demonstrated this, reporting pressure and volume changes of both the cathode and anode of a SSB at 25 °C during constant current cycling at C-rates of C/10 and C/4, respectively. In this scenario, a composite cathode composed of $LiCoO_2$, with a 1 wt%-$LiNb_{0.5}Ta_{0.5}O_3$ coating, and $Li_{10}GeP_2S_{12}$ (LGPS) additive was used along with an LGPS solid electrolyte inside the dilatometer assembly. The anode consisted of an indium foil.[161] Significant thickness and pressure changes occurred during SSB cycling. The volume expansion of the $LiCoO_2$ cathode, and the volume expansion during the solid-state reaction from tetragonal indium to the cubic $InLi_{1-x}$ phase were mostly accountable for the observed thickness/pressure variations of the SSB cell. The volume changes at the $Li_4Ti_5O_{12}$ anode were found to be minimal in comparison. At higher C-rate less capacity was obtained which lead to lower thickness and pressure changes. It was suggested that the decrease in capacity at higher C-rates was due to irreversible processes at the electrode/electrolyte interface and particle contact loss due to the "breathing" of the SSB. The work of Zhang et al.[161] can be built on by using different electrode compositions in the same dilatometry

Batteries & Supercaps

Reviews
doi.org/10.1002/batt.202100027

Chemistry
Europe
European Chemical
Societies Publishing

assembly to investigate the volume expansion of different SSB active materials. At the time of this review, research of dilatometry during operation of SSBs is very limited, and most dilatometric studies of SSBs focus on the processing stage. It seems the potential to use dilatometry to reveal pressure and volume changes of SSB pellets during operation has not yet been fully realised and could contribute to the understanding of the degradation of these materials.

SSB research contains the most diverse use of dilatometer models for experimentation when compared to other electrochemical devices. Sintering temperatures can exceed 600 °C; Baek et al. stated that a sintered body that can function as an electrolyte cannot be formed at temperatures below 400 °C.[162] Push rod dilatometers allow measurements to be taken between 0 °C and 1200 °C.[157,159,160] Other dilatometers are incapable of operating within this temperature range. For instance, the ECD-3 model has an operating temperature range of −20 °C to 70 °C.

2.4. Dilatometric Characterisation of Li−S Batteries

Li−S batteries have the potential to supersede LiBs owing to their higher gravimetric energy density capabilities. However, Li−S batteries present various complications, such as the dissolution of active material in the electrolyte phase and large volume changes of the cathode.[163–165] Two main drawbacks of Li−S batteries include lithiation from sulfur to Li sulphide in Li−S battery cathodes causing up to 80% volume expansion and shuttling of polysulfide compounds, in turn leading to an irreversible contraction of Li−S battery cathodes.[166–168]

The binder in sulfur electrodes plays a pivotal role in the electrochemical performance of Li−S batteries. The binder that provides better mechanical strength is likely to reduce the thickness variation of sulfur electrodes during cycling. Lemarie et al.[169] compared the thickness variation of three sulfur electrodes composed of three different binders; PVdF, CMC and cationic polyelectrolyte (PDDA). They found the polyelectrolyte-based electrode displayed the lowest irreversible thickness contraction of ~16% compared to ~22% and ~31% for CMC and PVdF respectively, during the initial discharge cycle (sulfur dissolution). These results were averaged from three dilatometry measurements per formulation and suggest that the structural integrity is highest for PDDA, followed by CMC and PVdF. The electrode with the least thickness variation is ultimately likely to have the most prolonged cycle life in the Li−S battery. As with previously discussed examples that take advantage of coupled characterisation with dilatometry, this study uses in situ dilatometry in conjunction with electrochemical AE and in-situ synchrotron X-ray tomography. In situ X-ray CT analysis was focused on the 1st discharge of the CMC and PDDA electrodes, as this was when large irreversible electrode morphological changes occurred as suggested from the previous ECD and AE measurements.

Li et al. explored the lithiation/delithiation and polysulfide dissolution-induced dimensional changes in Li−S cathodes during charge/discharge.[166] Two Li−S cathode materials were

investigated: activated carbon cloth (ACC) which boasted a very high specific surface area, and ACC impregnated with Li_2S (ACC@Li_2S). It was stated that ACC can reversibly store Li through adsorption, but not through redox processes. Whereas ACC@Li_2S could undergo both capacitive and faradaic processes to store Li. The ACC electrode was used as a control for the dilatometry measurements. An irreversible contraction was recorded due to the continuous dissolution of polysulfide compounds into the electrolyte during cycling. The findings shed new light on the failure mechanism of Li−S cathodes, and, in doing so, further explain the origin of the poor cycle-life of these batteries. Based on these new insights, the cycle-life and health of Li−S batteries can be improved by partially controlling the dimensional changes occurring in the materials, in order to mitigate detrimentally large volume expansions. Although the reversible dimensional changes cannot be avoided entirely, the irreversible dimensional changes can be reduced by preventing the loss of active material during cycling, and in turn, improving the cycle-life of Li−S batteries.[166]

A major concern in Li−S batteries is Li dendrite formation at the surface of the Li electrode which can ultimately lead to cell failure. Kuzmina et al. investigated whether ECD can be adopted to investigate Li dendrite growth in a Li−S modified Swagelok® type stainless steel cell equipped with an LVDT.[170] It was found that ECD can not only reveal Li dendrite formation at early stages but also quantify their growth rate. In the early stages of cycling, no significant changes in electrode thickness were recorded, however, after SEI formation, an increase in Li electrode thickness at a nearly constant rate was recorded as new Li dendrites grew progressively. The increase in electrode thickness coincided with a slight decrease in voltage which is to be expected as Li metal becomes electrochemically inactive.

At the time of this review, there is a general lack of research into the dimensional changes in a Li−S battery using ECD. However, there is potential to use ECD to investigate the dimensional changes of sulfur electrodes composed of different binders, the impact of polysulfide dissolution on the dimensional changes of Li−S cathodes and the dimensional changes associated with dendrite formation. Ultimately, Li is one of the most promising anode materials in a rechargeable battery as it offers a high theoretical specific capacity (3860 mA h g^{-1}) and the large negative standard redox potential in the electrochemical series.[171] The work of Kuzima et al. could be adapted for LIB chemistries that utilise a Li electrode to overcome limitations in dendrite growth at Li electrodes so that impressive energy densities can be realised in next generation rechargeable batteries.

3. Summary and Outlook

Dilatometry is a useful tool for monitoring thickness changes and demonstrating that irreversible dimensional changes can be reduced by, for example, preventing the loss of active material during operation. It is a tool capable of showing alterations in irreversible dilation depending on electrode design and experimental set-up and thus is a useful technique

Batteries & Supercaps

Reviews
doi.org/10.1002/batt.202100027

Chemistry Europe
European Chemical
Societies Publishing

for assessing battery stability and lifetime. There are multiple different dilatometry set-ups, which include instruments capable of monitoring single electrode expansion and those capable of monitoring electrode stacks. However, resolution can reduce as the measured volume is increased. While dilatometry is a powerful technique to probe the dimensional changes of electrodes during galvanostatic cycling, there are degradation mechanisms such as particle cracking and chemical material changes that do not contribute to thickness changes but can nonetheless lead to capacity fading. In addition, it can be difficult to decouple what is causing the thickness variations recorded. Multiple degradation mechanisms can occur at the same time. For instance, volume expansion that occurs due to electrode delamination can only be observed using other microscopy techniques. Also, expansion and contraction of an electrode during operation is expected to occur even in relatively healthy cells. For instance, graphite anodes in LiBs dilate during ion intercalation and contract during ion deintercalation. Therefore, these volume changes are not necessarily a reflection of any degradation mechanism.

When choosing an instrument for dilatometric studies, three main questions should be asked. Firstly, is the resolution sufficient? This is particularly important for studying cathode materials that undergo constant but less significant volume changes than their anode counterparts. Secondly, does the instrument provide a suitable working temperature range? This review has shown that different models are selected when studying materials at temperatures higher than 700 °C. Thirdly, is the cell hermetically sealed? The cell has to be assembled in a way to avoid moisture or air contamination, particularly for sensitive cathode materials.

In the future, there may be more research on metal-air batteries and materials used in fuel cells. There are some dilatometric studies into anodes used in Zinc-air batteries, and thickness changes of sealants used in solid oxide fuel cells (SOFCs) at temperatures exceeding 700 °C, but dilatometric research with these devices is limited.[172–174] Nonetheless, thickness change measurements are not limited to dilatometry. Micrometres and strain gauges can also be used to measure the thickness changes of single electrode and full cell arrangements.[143,175–182] Ex-situ dilatometric measurements of thickness changes after cycling have also been carried out on electrochemical devices.[183,184] A drawback of making these measurements after cycling is that it is not possible to deduce the nature of the measured dimensional changes. For instance, reversible thickness changes can occur as a result of particular phase transitions that can occur at certain voltages. Lee et al. evaluated the dimensional changes of an entire $LiCoO_2$ pouch cell during cycling using a thickness gauge; they found that the battery expansion is comprised of two elements; an initial formation of SEI causing an irreversible increase in thickness, and one which is reversible and follows battery state of charge, expanding with charging. The volume changes to the anode active material during cycling were found to be approximately 2 % of the total initial battery thickness; the lithium cobalt oxide did not show significant volume changes upon Li

intercalation.[185] However, the dilatometers referenced in this review display a higher resolution than a thickness gauge.

Lee et al. have argued that dilatometry experiments cannot distinguish between electrode expansion and displacement due to gas evolution, and that neutron imaging is capable of detecting these differences if the gas accumulated is large enough due to the large change in density and transmission through the tested material.[186] Modern dilatometer design can effectively manage and mitigate unwanted pressure build-up due to gas evolution.

This review has considered and discussed a variety of published studies that use dilatometry to investigate the volume changes undergone by materials used in electrochemical devices, and the impact these changes can have on the performance of the device. Other techniques such as X-ray CT,[33] solid-state NMR,[81] and X-ray diffraction[152] can be used in conjunction with dilatometry to corroborate and explain the dimensional changes recorded, enhance understanding of the impacts of these changes, and inform mitigation to improve performance. Dilatometry is useful for laboratory use, but less suited to real-world application since integration of a dilatometer in a battery system is difficult and potentially destructive. Strain gauges may show more promise for real-world application given that they have been used in a laboratory setting to evaluate a matrix of LiBs on battery ageing during operation.[181] Interestingly, most studies reviewed in this work investigate thickness variations during standard galvanostatic conditions with moderately slow C-rates; there is a lack of dilatometric studies at high C-rates, as well as studies on ageing, safety and abusive conditions apart from Li plating. Perhaps this is due to limitations in design in the current state-of-the-art commercial dilatometers and challenges with in-house constructed dilatometers, though this is a noticeable gap in the literature that would provide valuable information about the performance of batteries under more realistic cycling and ageing regimes.

There are multiple degradation mechanisms at play in the ageing of a cell and learning about how to predict which one(s) (or combinations) are most critical in particular conditions is vital to understanding and mitigating degradation, especially for ostensibly similar cells.[6] Progress in dilatometric investigations of electrode dilation/contraction in electrochemical devices can inform understanding of structural changes during electrode phase transitions and their contribution to the overall electrode dimensional changes. A greater understanding of these electrode dynamics is required to overcome limitations in current density, battery lifetime and capacity fade. The acceleration in the number of papers published on this topic is evidence of the increased focus on dilatometry as a diagnostic tool and the advancement of the technique in recent years. In addition, more studies are using dilatometry in tandem with other characterisation tools to further enhance our understanding of the structural changes taking place in the materials that make up electrochemical devices.

In conclusion, the outlook for the increased use of dilatometry in battery research is promising. Although there is a plethora of research using dilatometry in conventional anode materials such as graphite and silicon and commonly used

Batteries & Supercaps

Reviews
doi.org/10.1002/batt.202100027

Chemistry Europe
European Chemical
Societies Publishing

cathode materials such as LCO, there is scope for in-situ ECD to be used to assess next generation anode and cathode materials. There is a growing consensus of the need to migrate from the current state-of-the-art layered NMC cathodes to stoichiometries with lower cobalt content. For instance, in October 2019, The Faraday Institution, the UK's independent institute for electrochemical energy storage science and technology, launched the FUTURECAT, NEXTRODE and CATMAT programmes to develop and deploy next generation Li-ion electrodes and the NEXTGENNA programme that looks to develop novel electrode materials for NiBs. Dilatometry can be used to evaluate novel compositions of NMC electrodes in LiBs and innovative electrode materials in NiBs.

Acknowledgements

Conflict of Interest

The authors declare no conflict of interest.

[1] S. Yoda, K. Ishihara, *J. Power Sources* **1997**, *68*, 3–7.
[2] S. G. Chalk, J. F. Miller, *J. Power Sources* **2020**, *159*, 73–80.
[3] X. Hu, N. Murgovski, L. Johannesson, B. Egardt, *Appl. Energy* **2013**, *111*, 1001–1009.
[4] A. V Llewellyn, A. Matruglio, D. J. L. Brett, R. Jervis, P. R. Shearing, *Condens. Matter* **2020**, *5*, 75.
[5] C. Bommier, W. Chang, J. Li, S. Biswas, G. Davies, J. Nanda, D. Steingart, *J. Electrochem. Soc.* **2020**, *167*, 020517.
[6] M. G. Boebinger, J. A. Lewis, S. E. Sandoval, M. T. McDowell, *ACS Energy Lett.* **2020**, *5*, 335–345.
[7] A. C. Marschilok, A. M. Bruck, A. Abraham, C. A. Stackhouse, K. J. Takeuchi, E. S. Takeuchi, M. Croft, J. W. Gallaway, *Phys. Chem. Chem. Phys.* **2020**, *22*, 20972–20989.
[8] W. Zhao, J. Yi, P. He, H. Zhou, *Electrochem. Energy Rev.* **2019**, *2*, 574–605.
[9] N. Azimi, Z. Xue, S. S. Zhang, Z. Zhang, *Rechargeable Lithium Batteries, From Fundamentals to Applications* (Ed. A. A. Franco), Woodhead Publshing, **2015**.
[10] S. Evers, L. F. Nazar, *Acc. Chem. Res.* **2013**, *46*, 1135–1143.
[11] C. Tan, S. Randjbar Daemi, D. J. L. Brett, P. R. Shearing, *ECS Trans.* **2017**, *77*, 447–455.
[12] J. Robinson, K. Xi, R. V. Kumar, A. C. Ferrari, H. Au, M.-M. Titirici, A. Parra Puerto, A. Kucernak, S. D. S. Fitch, N. Garcia-Araez, *J. Phys. E* **2020**, *2*, 0–31.
[13] S. S. Zhang, *J. Power Sources* **2013**, *231*, 153–162.
[14] R. Kumar, J. Liu, J. Y. Hwang, Y. K. Sun, *J. Mater. Chem. A* **2018**, *6*, 11582–11605.
[15] T. Ould Ely, D. Kamzabek, D. Chakraborty, M. F. Doherty, *ACS Appl. Mater. Interfaces* **2018**, *1*, 1783–1814.
[16] Y. Jiang, F. Chen, Y. Gao, Y. Wang, S. Wang, Q. Gao, Z. Jiao, B. Zhao, Z. Chen, *J. Power Sources* **2017**, *342*, 929–938.
[17] P. Barai, A. Mistry, P. P. Mukherjee, *Extrem. Mech. Lett.* **2016**, *9*, 359–370.
[18] M. Li, Z. Wang, J. Fu, K. Ma, E. Detsi, *Acta Mater.* **2019**, *164*, 52–56.
[19] B. Karmakar, P. Kundu, S. Jana, R. N. Dwivedi, *J. Am. Ceram. Soc.* **2002**, *85*, 2572–2574.
[20] F. B. Spingler, W. Wittmann, J. Sturm, B. Rieger, A. Jossen, *J. Power Sources* **2018**, *393*, 152–160.
[21] G. Bohn, J. Taub, A. Linke, S. Bayer, D. Oeser, A. Ziegler, P. Ettl, A. Ackva, *IOP Conf. Ser. Earth Environ. Sci.* **2019**, *281*, 012030.
[22] R. Küchler, T. Bauer, M. Brando, F. Steglich, *Rev. Sci. Instrum.* **2012**, *83*, 095102.
[23] M. O. Steinitz, J. Genossar, W. Schnepf, D. A. Tindall, *Rev. Sci. Instrum.* **1986**, *57*, 297–298.
[24] G. M. Schmiedeshoff, A. W. Lounsbury, D. J. Luna, S. J. Tracy, A. J. Schramm, S. W. Tozer, V. F. Correa, S. T. Hannahs, T. P. Murphy, E. C. Palm, A. H. Lacerda, S. L. Bud'Ko, P. C. Canfield, J. L. Smith, J. C. Lashley, J. C. Cooley, *Rev. Sci. Instrum.* **2006**, *77*, 123907.
[25] J. J. Neumeier, R. K. Bollinger, G. E. Timmins, C. R. Lane, R. D. Krogstad, J. Macaluso, *Rev. Sci. Instrum.* **2008**, *79*, 1–8.
[26] S. Jun, Y. J. Nam, H. Kwak, K. T. Kim, D. Y. Oh, Y. S. Jung, *Adv. Funct. Mater.* **2020**, *30*, 2002535.
[27] S. H. Jung, U. H. Kim, J. H. Kim, S. Jun, C. S. Yoon, Y. S. Jung, Y. K. Sun, *Adv. Energy Mater.* **2020**, *10*, 1903360.
[28] M. Hahn, O. Barbieri, F. P. Campana, R. Kotz, R. Gallay, *Appl. Phys.* **2006**, *82*, 633–638.
[29] M. Winter, G. H. Wrodnigg, J. O. Besenhard, W. Biberacher, P. Novák, *J. Electrochem. Soc.* **2000**, *147*, 2427.
[30] D. Sauerteig, S. Ivanov, H. Reinshagen, A. Bund, *J. Power Sources* **2017**, *342*, 939–946.
[31] M. Bauer, J. V. Persson, M. A. Danzer, M. Wachtler, H. Stowe, *J. Power Sources* **2016**, *317*, 93–102.
[32] G. Jeong, S. M. Lee, N. S. Choi, Y.-U. Kim, C. K. Lee, *Electrochim. Acta* **2011**, *56*, 5095–5101.
[33] H. Michael, F. Iacoviello, T. Heenan, A. Llewellyn, J. Weaving, R. Jervis, D. Brett, P. R. Shearing, *J. Electrochem. Soc.* **2021**, *168*, 010507.
[34] S. Ivanov, D. Sauerteig, A. Dimitrova, S. Krischok, A. Bund, *J. Power Sources* **2020**, *457*, 228020.
[35] R. Fu, M. Xiao, S. Y. Choe, *J. Power Sources* **2013**, *224*, 211–224.
[36] M. Bauer, B. Rieger, S. Schindler, P. Keil, M. Wachtler, M. A. Danzer, A. Jossen, *J. Energy Storage* **2017**, *10*, 1–10.
[37] S. Choi, T. Kwon, A. Coskun, *Science* **2017**, *357*, 279–283.
[38] A. Magasinski, B. Zdyrko, I. Kovalenko, B. Hertzberg, R. Burtovyy, C. F. Huebner, T. F. Fuller, I. Luzinov, G. Yushin, *ACS Appl. Mater. Interfaces* **2010**, *2*, 3004–3010.
[39] S. Kalnaus, K. Rhodes, C. Daniel, *J. Power Sources* **2011**, *196*, 8116–8124.
[40] W. Brehm, A. L. Santhosha, Z. Zhang, C. Neumann, A. Turchanin, M. Seyring, M. Rettenmayr, J. R. Buchheim, P. Adelhelm, *J. Power Sources* **2020**, *6*, 100031.
[41] C. Wang, A. J. Appleby, F. E. Little, *J. Electroanal. Chem.* **2002**, *519*, 9–17.
[42] J. P. Pender, G. Jha, D. H. Youn, J. M. Ziegler, I. Andoni, E. J. Choi, A. Heller, B. S. Dunn, P. S. Weiss, R. M. Penner, C. B. Mullins, *ACS Nano* **2020**, *14*, 1243–1295.
[43] X. Song, K. Kinoshita, *J. Electrochem. Soc.* **1995**, *142*, 3297–3302.
[44] T. Tran, K. Kinoshita, *J. Electroanal. Chem.* **1995**, *386*, 221–224.
[45] L. Zhang, C. Chen, *Prog. Chem.* **2011**, *23*, 275–283.
[46] T. Ohzuku, N. Matoba, K. Sawai, *J. Power Sources* **2001**, *97–98*, 73–77.
[47] X. Y. Song, K. Kinoshita, *J. Electrochem. Soc.* **1996**, *143*, L120–L123.
[48] G. V. Zhuang, P. N. Ross, A. Augustsson, M. Herstedt, K. Edstro, J. Nordgren, A. L. Source, L. Berkeley, M. S. Division, L. Berkeley, *Phys. Chem. Chem. Phys.* **2004**, *6*, 4185–4189.
[49] W. Biberacher, A. Lerf, J. O. Besenhard, H. Mohwald, T. Butz, *Mat. Res. Bull.* **1982**, *17*, 1385–1392.
[50] J. O. Besenhard, J. Yang, M. Winter, *J. Power Sources* **1997**, *68*, 87–90.
[51] J. Yang, M. Winter, J. O. Besenhard, *Solid State Ionics* **1996**, *90*, 281–287.
[52] J. O. Besenhard, M. Winter, J. Yang, W. Biberacher, *J. Power Sources* **1995**, *54*, 228–231.
[53] M. Hahn, O. Barbieri, R. Gallay, R. Kötz, *Carbon N. Y.* **2006**, *44*, 2523–2533.
[54] M. Hahn, H. Buqa, P. W. Ruch, D. Goers, M. E. Spahr, J. Ufheil, P. Novák, R. Kötz, *Electrochem. Solid-State Lett.* **2008**, *11*, A151.
[55] M. M. Hantel, R. Nesper, A. Wokaun, R. Kötz, *Electrochim. Acta* **2014**, *134*, 459–470.
[56] S. Schweidler, L. De Biasi, A. Schiele, P. Hartmann, T. Brezesinski, J. Janek, *J. Phys. Chem. C* **2018**, *122*, 8829–8835.

Batteries & Supercaps

Reviews

doi.org/10.1002/batt.202100027

Chemistry
Europe

European Chemical
Societies Publishing

[57] D. Sauerteig, S. Ivanov, H. Reinshagen, A. Bund, *J. Power Sources* **2017**, *342*, 939–946.

[58] J. B. Siegel, A. G. Stefanopoulou, P. Hagans, Y. Ding, D. Gorsich, *J. Electrochem. Soc.* **2013**, *160*, A1031–A1038.

[59] M. Winter, J. O. Besenhard, M. E. Spahr, P. Novák, *Adv. Mater.* **1998**, *10*, 725–763.

[60] M. Winter, G. H. Wrodnigg, J. O. Besenhard, W. Biberacher, P. Novák, *J. Electrochem. Soc.* **2000**, *147*, 2427.

[61] J. Huesker, L. Froböse, A. Kwade, M. Winter, T. Placke, *Electrochim. Acta* **2017**, *257*, 423–435.

[62] M. R. Wagner, P. R. Raimann, A. Trifonova, K. C. Möller, J. O. Besenhard, M. Winter, *Anal. Bioanal. Chem.* **2004**, *379*, 272–276.

[63] H.-D. Yoo, J.-H. Ryu, S.-H. Park, Y.-W. Park, B.-H. Ka, S.-M. Oh, *J. Electrochem. Sci. Technol.* **2011**, *2*, 45–50.

[64] F. Grimsmann, F. Brauchle, T. Gerbert, A. Gruhle, M. Knipper, J. Parisi, *J. Energy Storage* **2017**, *12*, 132–137.

[65] M. Kerlau, M. Marcinek, R. Kostecki, *J. Power Sources* **2007**, *174*, 1046–1051.

[66] Y. Qi, S. J. Harris, *J. Electrochem. Soc.* **2010**, *157*, A741.

[67] H. Wu, Y. Cui, *Nano Today* **2012**, *7*, 414–429.

[68] U. Kasavajjula, C. Wang, A. J. Appleby, *J. Power Sources* **2007**, *163*, 1003–1039.

[69] L. F. Cui, R. Ruffo, C. K. Chan, H. Peng, Y. Cui, *Nano Lett.* **2009**, *9*, 491–495.

[70] M. J. Chon, V. A. Sethuraman, A. McCormick, V. Srinivasan, P. R. Guduru, *Phys. Rev. Lett.* **2011**, *107*, 1–4.

[71] M. T. McDowell, S. W. Lee, J. T. Harris, B. A. Korgel, C. Wang, W. D. Nix, Y. Cui, *Nano Lett.* **2013**, *13*, 758–764.

[72] B. Key, M. Morcrette, J. M. Tarascon, C. P. Grey, *J. Am. Chem. Soc.* **2011**, *133*, 503–512.

[73] M. T. Mcdowell, S. W. Lee, W. D. Nix, Y. Cui, *Adv. Mater.* **2013**, *25*, 4966–4985.

[74] Z. Karkar, T. Jaouhari, A. Tranchot, D. Mazouzi, D. Guyomard, B. Lestriez, L. Roué, *J. Power Sources* **2017**, *371*, 136–147.

[75] S. Zhang, *npj Comput. Mater.* **2017**, *3*, 1–10.

[76] Y. Nam, Y. Kim, J. Soo, J. Ho, K. Jae, C. Yun, D. Jun, C. Wan, Y. Jun, *J. Power Sources* **2010**, *195*, 6031–6036.

[77] A. Guerfi, P. Charest, M. Dontigny, J. Trottier, M. Lagacé, P. Hovington, A. Vijh, K. Zaghib, *J. Power Sources* **2011**, *196*, 5667–5673.

[78] P. Hovington, M. Dontigny, A. Guer, J. Trottier, M. Lagacé, A. Mauger, C. M. Julien, K. Zaghib, *J. Power Sources* **2014**, *248*, 457–464.

[79] D. M. Piper, J. H. Woo, S. Son, S. C. Kim, K. H. Oh, S. Lee, *Adv. Mater.* **2014**, *26*, 3520–3525.

[80] M. Holzapfel, H. Buqa, L. J. Hardwick, M. Hahn, W. Andreas, W. Scheifele, P. Nov, C. Veit, F. Petrat, *Electrochim. Acta* **2006**, *52*, 973–978.

[81] T. Kim, J. E. Soc, T. Kim, S. Park, S. M. Oh, *J. Electrochem. Soc.* **2007**, *154*, A1112–A1117.

[82] M. M. Hantel, V. Presser, J. K. McDonough, G. Feng, P. T. Cummings, Y. Gogotsi, R. Kötz, *J. Electrochem. Soc.* **2012**, *159*, A1897–A1903.

[83] S. Park, T. Kim, S. M. Oh, *Electrochem. Solid-State Lett.* **2007**, *10*, 142–145.

[84] J. L. Gómez Cámer, J. Morales, L. Sánchez, P. Ruch, S. H. Ng, R. Kötz, P. Novák, *Electrochim. Acta* **2009**, *54*, 6713–6717.

[85] J. Sub, W. Choi, K. Young, D. Byun, J. Lim, J. Kee, *J. Power Sources* **2013**, *244*, 521–526.

[86] Y. Lee, T. Lee, J. Hong, J. Sung, N. Kim, Y. Son, J. Ma, S. Y. Kim, J. Cho, *Adv. Funct. Mater.* **2020**, *30*, 2004841.

[87] S. Chae, S. Park, K. Ahn, G. Nam, T. Lee, J. Sung, N. Kim, J. Cho, *Energy Environ. Sci.* **2020**, *13*, 1212–1221.

[88] D. Y. W. Yu, M. Zhao, H. E. Hoster, *ChemElectroChem* **2015**, *2*, 1090–1095.

[89] A. Tranchot, H. Idrissi, *J. Power Sources* **2016**, *330*, 253–260.

[90] P. Lee, M. H. Tahmasebi, T. Tan, S. Ran, S. T. Boles, D. Y. W. Yu, *Mater. Today* **2019**, *12*, 297–302.

[91] T. Tan, P. K. Lee, N. Zettsu, K. Teshima, D. Y. W. Yu, *J. Power Sources* **2020**, *453*, 227874.

[92] N. Ding, J. Xu, Y. Yao, G. Wegner, I. Lieberwirth, C. Chen, *J. Power Sources* **2009**, *192*, 644–651.

[93] T. Yoon, C. C. Nguyen, D. M. Seo, B. L. Lucht, *J. Electrochem. Soc.* **2015**, *162*, A2325–A2330.

[94] S. Goriparti, E. Miele, F. De Angelis, E. Di Fabrizio, R. Proietti Zaccaria, C. Capiglia, *J. Power Sources* **2014**, *257*, 421–443.

[95] H. Kim, M. Seo, M. H. Park, J. Cho, *Angew. Chem. Int. Ed.* **2010**, *49*, 2146–2149; *Angew. Chem.* **2010**, *122*, 2192–2195.

[96] Z. Karkar, D. Mazouzi, C. R. Hernandez, D. Guyomard, L. Roué, B. Lestriez, *Electrochim. Acta* **2016**, *215*, 276–288.

[97] N. Yuca, Ü. Çolak, *Electrochim. Acta* **2016**, *222*, 1538–1544.

[98] H. Zhao, N. Yuca, Z. Zheng, Y. Fu, V. S. Battaglia, G. Abdelbast, K. Zaghib, G. Liu, *ACS Appl. Mater. Interfaces* **2015**, *7*, 862–866.

[99] G. Lenze, F. Röder, H. Bockholt, W. Haselrieder, A. Kwade, U. Krewer, *J. Electrochem. Soc.* **2017**, *164*, A1223–A1233.

[100] C. Meyer, H. Bockholt, W. Haselrieder, A. Kwade, *J. Mater. Process. Technol.* **2017**, *249*, 172–178.

[101] C. F. Oladimeji, P. L. Moss, M. H. Weatherspoon, *Adv. Chem.* **2016**, *2016*, 7395060.

[102] T. M. M. Heenan, A. Wade, C. Tan, J. E. Parker, D. Matras, A. S. Leach, J. B. Robinson, A. Llewellyn, A. Dimitrijevic, R. Jervis, P. D. Quinn, D. J. L. Brett, P. R. Shearing, *Adv. Energy Mater.* **2020**, *10*, 2002655.

[103] S. Chae, M. Ko, K. Kim, K. Ahn, J. Cho, *Joule* **2017**, *1*, 47–60.

[104] A. Mukhopadhyay, B. W. Sheldon, *Prog. Mater. Sci.* **2014**, *63*, 58–116.

[105] S. Wang, Q. Duan, J. Lei, D. Y. W. Yu, *J. Power Sources* **2020**, *468*, 228365.

[106] B. Gendensuren, E. Oh, *J. Power Sources* **2018**, *384*, 379–386.

[107] N. Jäckel, V. Dargel, N. Shpigel, S. Sigalov, M. D. Levi, L. Daikhin, D. Aurbach, V. Presser, *J. Power Sources* **2017**, *371*, 162–166.

[108] H. Park, D. G. Lee, D. J. Chung, M. Sohn, C. Park, *Korean Chem. Soc.* **2019**, *40*, 248–253.

[109] H. S. Yang, S. H. Kim, A. G. Kannan, S. K. Kim, C. Park, D. W. Kim, *Langmuir* **2016**, *32*, 3300–3307.

[110] X. Li, P. W. Bonn, *Appl. Phys. Lett.* **2000**, *77*, 2572–2574.

[111] J. S. Kim, W. Choi, K. Y. Cho, D. Byun, J. Lim, J. K. Lee, *J. Power Sources* **2013**, *244*, 521–526.

[112] H.-K. Kim, K. C. Roh, K.-B. Kim, *J. Electrochem. Soc.* **2015**, *162*, A2308–A2312.

[113] R. Yi, M. L. Gordin, D. Wang, *Nanoscale* **2016**, *8*, 1834–1848.

[114] H. Yu, E. Lett, H. Yu, K. Hong, M. Sung, S. Lee, Y. Sheem, *J. Electrochem. Soc.* **2013**, *2*, A10–A13.

[115] Y. Wang, C. Malveau, D. Rochefort, *Energy Storage Mater.* **2019**, *20*, 80–88.

[116] Y. Sun, Z. W. Seh, J. Sun, Y. Sun, G. Zheng, Z. W. Seh, N. Liu, S. Wang, J. Sun, *Chem* **2016**, *1*, 287–297.

[117] D. Aurbach, B. Markovsky, I. Weissman, E. Levi, Y. Ein-Eli, *Electrochim. Acta* **1999**, *45*, 67–86.

[118] N. Nitta, G. Yushin, *Part. Part. Syst. Charact.* **2014**, *31*, 317–336.

[119] N. Nitta, F. Wu, J. T. Lee, G. Yushin, *Biochem. Pharmacol.* **2015**, *18*, 252–264.

[120] Y. Li, S. Wang, P. Lee, J. He, D. Y. W. Yu, *J. Power Sources* **2017**, *366*, 226–232.

[121] H. Lv, S. Qiu, G. Lu, Y. Fu, X. Li, C. Hu, J. Liu, *Electrochim. Acta* **2015**, *151*, 214–221.

[122] S. Wang, X. Yang, P. Lee, A. L. Rogach, D. Y. W. Yu, *Chem. Mater.* **2019**, *31*, 2469–2475.

[123] S. Wang, P. Lee, X. Yang, A. L. Rogach, A. R. Armstrong, D. Y. W. Yu, *Mater. Today* **2018**, *9*, 295–302.

[124] K. Ma, J. S. Corsi, J. Fu, E. Detsi, *ACS Appl. Nano Mater.* **2018**, *1*, 541–546.

[125] Y. Ma, Y. Ma, G. Kim, T. Diemant, R. J. Behm, D. Geiger, U. Kaiser, A. Varzi, S. Passerini, *Adv. Energy Mater.* **2019**, *9*, 1902077.

[126] B. Rieger, S. Schlueter, S. V Erhard, J. Schmalz, G. Reinhart, A. Jossen, *J. Energy Storage* **2016**, *6*, 213–221.

[127] O. Dolotko, A. Senyshyn, M. J. Mühlbauer, K. Nikolowski, H. Ehrenberg, *J. Power Sources* **2014**, *255*, 197–203.

[128] P. K. Nayak, L. Yang, K. Pollok, F. Langenhorst, D. Aurbach, P. Adelhelm, *ChemElectroChem* **2019**, *6*, 2812–2819.

[129] R. A. House, G. J. Rees, M. A. Pérez-Osorio, J. J. Marie, E. Boivin, A. W. Robertson, A. Nag, M. Garcia-Fernandez, K. J. Zhou, P. G. Bruce, *Nat. Energy* **2020**, *5*, 777–785.

[130] K. Ariyoshi, H. Yamamoto, Y. Yamada, *Electrochim. Acta* **2018**, *260*, 498–503.

[131] M. Nagayama, K. Ariyoshi, Y. Yamamoto, T. Ohzuku, *J. Electrochem. Soc.* **2014**, *161*, A1388–A1393.

[132] X. Tian, X. Xu, L. He, Q. Wei, M. Yan, L. Xu, Y. Zhao, C. Yang, L. Mai, *J. Power Sources* **2014**, *255*, 235–241.

[133] J. Zhu, L. Cao, Y. Wu, Y. Gong, Z. Liu, H. E. Hoster, Y. Zhang, S. Zhang, S. Yang, Q. Yan, P. M. Ajayan, R. Vajtai, *Nano Lett.* **2013**, *13*, 5408–5413.

[134] J. Barker, O.-K. Chang, R. Koksbang, *J. Electrochem. Soc.* **1995**, *142*, 3246.

[135] D. W. Murphy, P. A. Christian, F. J. DiSalvo, J. N. Carides, J. V. Waszczak, *J. Electrochem. Soc.* **1981**, *128*, 2053–2060.

Batteries & Supercaps

Reviews
doi.org/10.1002/batt.202100027

Chemistry
Europe
European Chemical
Societies Publishing

[136] K. West, B. Zachau-Christiansen, T. Jacobsen, *Electrochim. Acta* **1983**, *28*, 1829–1833.

[137] J. Barker, *Electrochim. Acta* **1999**, *45*, 235–242.

[138] Z. J. Schiffer, J. Cannarella, C. B. Arnold, *J. Electrochem. Soc.* **2016**, *163*, A427–A433.

[139] H. Kim, J. Hong, G. Yoon, H. Kim, K. Y. Park, M. S. Park, W. S. Yoon, K. Kang, *Energy Environ. Sci.* **2015**, *8*, 2963–2969.

[140] B. Jache, J. O. Binder, T. Abe, P. Adelhelm, *Phys. Chem. Chem. Phys.* **2016**, *18*, 14299–14316.

[141] M. Goktas, C. Bolli, E. J. Berg, P. Novák, K. Pollok, F. Langenhorst, M. Roeder, O. Lenchuk, D. Mollenhauer, P. Adelhelm, *Adv. Energy Mater.* **2018**, *8*, 1702724.

[142] N. Karimi, A. Varzi, S. Passerini, *Electrochim. Acta* **2019**, *304*, 474–486.

[143] I. Escher, Y. Kravets, G. A. Ferrero, M. Goktas, P. Adelhelm, *Energy Technol.* **2020**, *2000880*.

[144] H. Alptekin, H. Au, A. Jensen, E. Olsson, M. Goktas, T. F. Headen, P. Adelhelm, Q. Cai, A. J. Drew, M.-M. Titirici, *ACS Appl. Mater. Interfaces* **2020**, *3*, 9918–9927.

[145] P. R. Abel, Y. Lin, T. De Souza, C. Chou, A. Gupta, J. B. Goodenough, G. S. Hwang, A. Heller, C. B. Mullins, *J. Phys. Chem. C* **2013**, *117*, 18885–18890.

[146] Y. Liu, Y. Xu, Y. Zhu, J. N. Culver, C. A. Lundgren, K. Xu, C. Wang, *ACS Nano* **2013**, *7*, 3627–3634.

[147] J. Qian, X. Wu, Y. Cao, X. Ai, H. Yang, *Angew. Chem. Int. Ed.* **2013**, *52*, 4633–4636; *Angew. Chem.* **2013**, *125*, 4731–4734.

[148] L. Liang, Y. Xu, C. Wang, L. Wen, Y. Fang, Y. Mi, M. Zhou, H. Zhao, Y. Lei, *Energy Environ. Sci.* **2015**, *8*, 2954–2962.

[149] W. Brehm, J. R. Buchheim, P. Adelhelm, *Energy Technol.* **2019**, *7*, 1900389.

[150] B. Qin, A. Schiele, Z. Jusys, A. Mariani, T. Diemant, X. Liu, T. Brezesinski, R. J. Behm, A. Varzi, S. Passerini, *ACS Appl. Mater. Interfaces* **2020**, *12*, 3697–3708.

[151] W. Wang, J. Zhang, D. Y. W. Yu, Q. Li, *J. Power Sources* **2017**, *364*, 420–425.

[152] T. Palaniselvam, M. Goktas, B. Anothumakkool, Y. N. Sun, R. Schmuch, L. Zhao, B. H. Han, M. Winter, P. Adelhelm, *Adv. Funct. Mater.* **2019**, *29*, 1–12.

[153] P. Thangavelu, B. Babu, A. Balducci, M. Hyein, I. Hasa, S. Passerini, A. L. Santhosha, M. Goktas, Y.-N. Sun, L. Zhao, B.-H. Han, P. Adelhelm, *Batteries & Supercaps* **2021**, *4*, 173–182.

[154] T. Palaniselvam, C. Mukundan, I. Hasa, A. L. Santhosha, M. Goktas, H. Moon, M. Ruttert, R. Schmuch, K. Pollok, F. Langenhorst, M. Winter, S. Passerini, P. Adelhelm, *Adv. Funct. Mater.* **2020**, *30*, 2004798.

[155] R. A. Jonson, P. J. McGinn, *Solid State Ionics* **2018**, *323*, 49–55.

[156] Y. Jin, P. J. McGinn, *J. Power Sources* **2011**, *196*, 8683–8687.

[157] T. Hupfer, E. C. Bucharskydr, K. G. Schelldr, M. J. Hoffmannprof, *Solid State Ionics* **2017**, *302*, 49–53.

[158] R. Shin, S. Ick, Y. Soo, Y. Do, H. Kim, S. Ryu, W. Pan, *Solid State Ionics* **2017**, *301*, 10–14.

[159] R. A. Jonson, P. J. Mcginn, *Solid State Ionics* **2018**, *323*, 49–55.

[160] B. Davaasuren, F. Tietz, *Solid State Ionics* **2019**, *338*, 144–152.

[161] W. Zhang, D. Schröder, T. Arlt, I. Manke, R. Koerver, R. Pinedo, D. A. Weber, J. Sann, W. G. Zeier, J. Janek, *J. Mater. Chem. A* **2017**, *5*, 9929–9936.

[162] S. W. Baek, J. M. Lee, T. Y. Kim, M. S. Song, Y. Park, *J. Power Sources* **2014**, *249*, 197–206.

[163] A. Yermukhambetova, C. Tan, S. R. Daemi, Z. Bakenov, *Nat. Publ. Gr.* **2016**, *6*, 1–9.

[164] C. Tan, T. M. M. Heenan, R. F. Ziesche, S. R. Daemi, J. Hack, M. Maier, S. Marathe, C. Rau, D. J. L. Brett, P. R. Shearing, *ACS Appl. Mater. Interfaces* **2018**, *1*, 5090–5100.

[165] J. Park, S.-H. Yu, Y.-E. Sung, *Nano Today* **2018**, *18*, 35–64.

[166] M. Li, Z. Wang, E. Detsi, *J. Electrochem. Soc.* **2020**, *167*, 050505.

[167] D. Liu, C. Zhang, G. Zhou, W. Lv, G. Ling, L. Zhi, *Adv. Sci.* **2018**, *5*, 1700270.

[168] O. Ogoke, G. Wu, X. Wang, A. Casimir, L. Ma, *J. Mater. Chem. A* **2017**, *5*, 448–469.

[169] Q. Lemarié, H. Idrissi, E. Maire, P. X. Thivel, F. Alloin, L. Roué, *J. Power Sources* **2020**, *477*, 228374.

[170] E. Kuzmina, E. Karaseva, A. Ivanov, D. Kolosnitsyn, S. Mochalov, R. V. Kumar, V. Kolosnitsyn, *Electrochim. Acta* **2019**, *327*, 135007.

[171] X. B. Cheng, C. Z. Zhao, Y. X. Yao, H. Liu, Q. Zhang, *Chem* **2019**, *5*, 74–96.

[172] M. Schmid, M. Willert-Porada, *Electrochim. Acta* **2018**, *260*, 246–253.

[173] S. Qi, N. M. Porotnikova, M. V Ananyev, A. V Kuzmin, V. A. Eremin, A. A. Pankratov, *Trans. Nonferrous Met. Soc. China* **2016**, *26*, 2916–2924.

[174] W. Zajac, L. Suescun, K. Świerczek, J. Molenda, *J. Power Sources* **2009**, *194*, 2–9.

[175] S. Waluś, G. Offer, I. Hunt, Y. Patel, T. Stockley, J. Williams, R. Purkayastha, *Energy Storage Mater.* **2018**, *10*, 233–245.

[176] Z. Du, Z. Du, R. A. Dunlap, M. N. Obrovac, *J. Electrochem. Soc.* **2014**, *161*, A1698–A1705.

[177] D. Mazouzi, N. Delpuech, Y. Oumellal, M. Gauthier, M. Cerbelaud, J. Gaubicher, N. Dupré, P. Moreau, D. Guyomard, L. Roué, B. Lestriez, *J. Power Sources* **2012**, *220*, 180–184.

[178] I. Soga, Y. Kinoshita, *J. Appl. Phys.* **2002**, *41*, 6616–6617.

[179] K. Y. Oh, J. B. Siegel, L. Secondo, S. U. Kim, N. A. Samad, J. Qin, D. Anderson, K. Garikipati, A. Knobloch, B. I. Epureanu, C. W. Monroe, A. Stefanopoulou, *J. Power Sources* **2014**, *267*, 197–202.

[180] B. Bitzer, A. Gruhle, *J. Power Sources* **2014**, *262*, 297–302.

[181] L. K. Willenberg, P. Dechent, G. Fuchs, D. U. Sauer, E. Figgemeier, *Sustain.* **2020**, *12*, 557.

[182] L. Hovestadt, K. Wildermann, A. Sahhary, R. Hanke-Rauschenbach, *J. Electrochem. Soc.* **2020**, *167*, 110540.

[183] Y. Park, N. S. Choi, S. Park, S. H. Woo, S. Sim, B. Y. Jang, S. M. Oh, S. Park, J. Cho, K. T. Lee, *Adv. Energy Mater.* **2013**, *3*, 206–212.

[184] X. He, J. Ren, L. Wang, W. Pu, C. Jiang, C. Wan, *J. Power Sources* **2009**, *190*, 154–156.

[185] J. H. Lee, H. M. Lee, S. Ahn, *J. Power Sources* **2003**, *121*, 833–837.

[186] J. B. Siegel, A. G. Stefanopoulou, P. Hagans, Y. Ding, D. Gorsich, *J. Electrochem. Soc.* **2013**, *160*, A1031–A1038.